PROGRESS TOWARDS THE INTELLIGENT CONTROL OF A POWERED TRANSFEMORAL PROSTHESIS

By

Huseyin Atakan Varol

Thesis

Submitted to the Faculty of the

Graduate School of Vanderbilt University in

partial fulfillment of the requirements

for the degree of

MASTER OF SCIENCE

in

Electrical Engineering

August, 2007

Nashville, Tennessee

Approved:

Professor Michael Goldfarb

Professor D. Mitch Wilkes

Professor George E. Cook

To my family

ACKNOWLEDGMENTS

First and foremost, I would like to thank my advisor Professor Michael Goldfarb for his inspiration, guidance, patience and encouragement throughout the duration of my thesis. He will be always a role model for my academic career. I would also like to express my appreciation and gratitude to Professor Mitch Wilkes and Professor George E. Cook for letting me to have them as members of my thesis committee.

This work would not have been possible without the grants of the National Science Foundation and the National Institutes of Health . Hereby, I greatly acknowledge both organisations for their support.

Thanks also go to all my colleagues at the Center for Intelligent Mechatronics. Post doctoral research associates Dr. Kevin Fite and Dr. Tom Withrow have been invaluable for their advice and assistance throughout my masters work. In particular, I would like to acknowledge Frank C. Sup for his contributions to my work and his outstanding advice and critique. I would also like to acknowledge David Slifer for his help during his summer internship. Moreover, I would like to thank David Braun for our informative and challenging technical discussions during the breaks.

I also wanted to thank those who shared joys and sorrows throuhgout my stay at Vanderbilt University: Barbaros Cetin, Duygun Erol, Erdem Erdemir, Jonathan E. Hunter, Mert Tugcu and Tamim I. Sookoor. I would like to express my sincere thanks to Gulnara Namyssova for always being with me and supporting me whenever I needed. Furthermore, I would like to thank my parents, Huseyin Selcuk Varol and Gungor Varol, and my brother Erkan Varol, whose love and trust I never lacked in my whole life.

TABLE OF CONTENTS

Page

APPENDIX

LIST OF FIGURES

Page

LIST OF TABLES

CHAPTER I

INTRODUCTION

1. Introduction

The evolution of the lower limb prosthesis over the recent decades has progressed from purely mechanical systems to systems that include microprocessor control. When evaluating the basic function of standard mechanical knee prostheses, Figure 1-1, their function is to provide mechanical damping in order to extract energy from the system and limit the flexion of the knee joint in the back swing to prevent a collision of the knee joint at full extension. These devices allow for restricted mobility of amputees and provide an abnormal gait pattern.

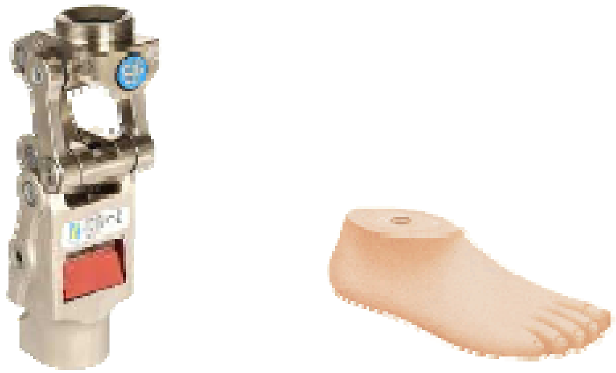

Figure 1-1. Standard lower limb prostheses including mechanical damping knee with locking and solid ankle cushioned heel (SACH) foot.

The current generation of lower limb prostheses, Figure 1-2, incorporate microprocessors to control either electromagnetic brakes or magnetic rheological fluid for the modulation of the damping in the knee throughout the gait cycle. The incorporation of spring elements in the ankle, Figure 1-3, provides some power return in the gait cycle, but is incapable of producing net power. The devices do provide users with increased mobility; however they still do not replace the power generation capabilities of the missing limb. The inability to deliver joint power significantly impairs the ability of lower limb prostheses to restore many locomotive functions, including walking up stairs and slopes, running, and jumping, all of which require significant net positive power at the knee joint, ankle joint, or both (Winter and Sienko 1988, Nadeau et al. 2003, Riener et al. 1999, Prilutsky et al. 1996, DeVita et al. 1996, Nagano et al. 1998, Jacobs et al. 1996). Further, although less obvious, even biomechanically normal walking requires positive power output at the knee joint and significant net positive power output at the ankle joint (Winter, 1991). Transfemoral amputees walking with passive prostheses have been shown to expend up to 60% more metabolic energy relative to healthy subjects during level walking (Waters et al. 1976) and exert as much as three times the affected-side hip power and torque (Winter 1991), presumably due to the absence of powered joints.

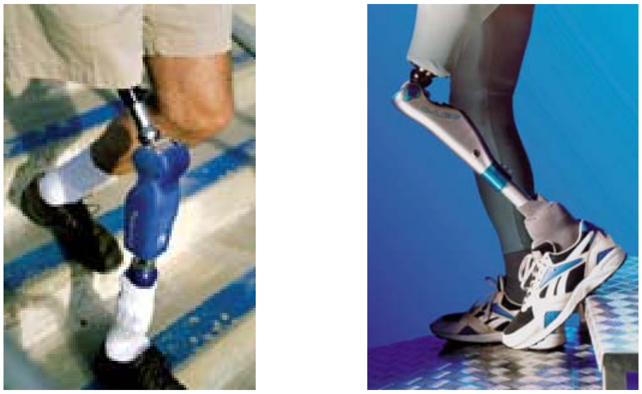

Figure 1-2. The Ossur Rheo knee (left) and the Otto Bock C-Leg (right) represent the cutting edge of microprocesser controlled damping prosthetic knees.

Figure 1-3. The Otto Bock Trias Foot represents a typical spring-action ankle.

A prosthesis with the capacity to deliver power at the knee and ankle joints would address these deficiencies, and would additionally enable the restoration of biomechanically normal locomotion. Such a prosthesis, however, would require 1) power generation capabilities comparable to an actual limb and 2) a control framework for generating required joint torques for locomotion while ensuring stable and coordinated interaction with the user and the environment.

2. Literature Survey

Prior work does exists on the development of powered knee transfemoral prostheses and powered ankle transtibial prostheses. Flowers (1973), Donath (1974), Flowers and Mann (1977), Grimes et al. (1977), Grimes (1979), Stein (1983), and Stein and Flowers (1988) developed a tethered electrohydraulic transfemoral prosthesis that consisted of a hydraulically actuated knee joint tethered to a hydraulic power source and off-board electronics and computation, Figure 1-4. They subsequently developed an "echo control" scheme for gait control, as described by Grimes et al. (1977), in which a modified knee trajectory from the sound leg is played back on the contralateral side.

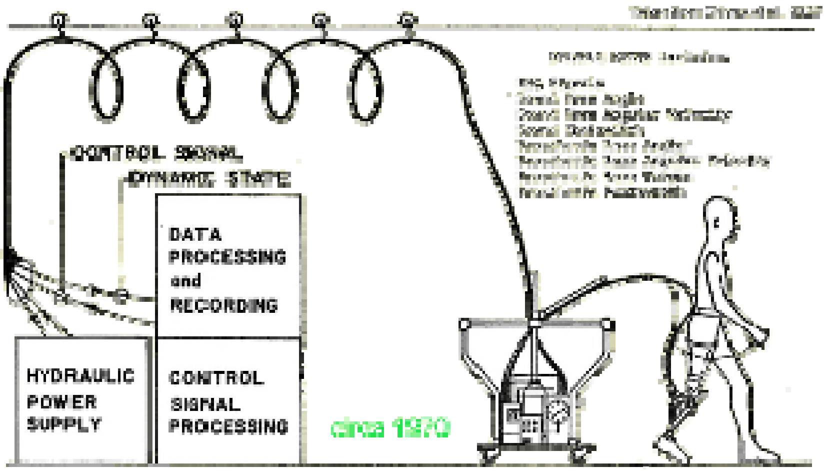

Figure 1-4. Flowers et al. (circa 1970's) developed a hydraulically actuated knee prosthesis that pioneered the use of active joints.

Specifically, Popovic and Schwirtlich (1988) report the development of a battery-powered active knee joint actuated by DC motors, Figure 1-5, together with a finite state knee controller that utilizes a robust position tracking control algorithm for gait control (Popovic et. al., 1995). With regard to powered ankle joints, Klute et al. (1998, 2000) describe the design of an active ankle joint using pneumatic McKibben actuators, although gait control algorithms were not described. Au et al. (2005) assessed the feasibility of an EMG based position control approach for a transtibial prosthesis. Finally, though no published literature exists, Ossur, a major prosthetics company based in Iceland, has announced the development of both a powered knee and a self-adjusting ankle. The latter, called the "Proprio Foot" (Figure 1-6) is not a true powered ankle, since it does not contribute power to gait, but rather is used to quasistatically adjust the angle of the ankle to better accommodate sitting and slopes. The powered knee, called the "Power Knee" (Figure 1-7), utilizes an echo control approach similar to the one described by Grimes et al. (1977).

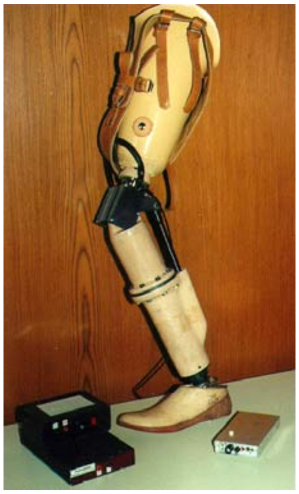

Figure 1-5. Electromagnetically actuated powered knee developed by Popovic with a battery pack.

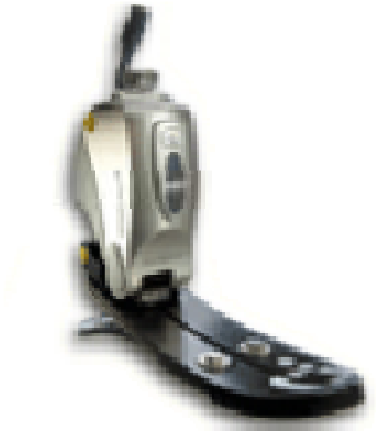

Figure 1-6. Ossur "Proprio" foot actively positions the foot for increased functionality.

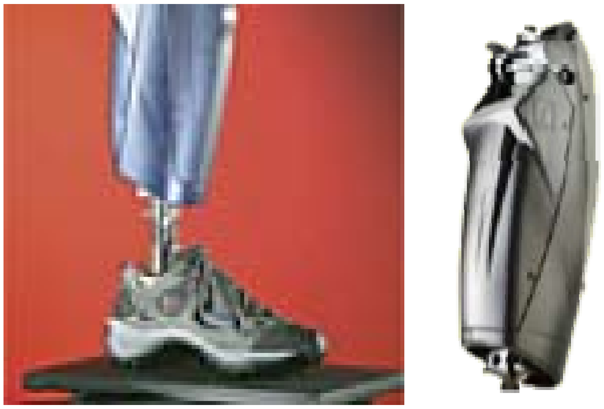

Figure 1-7. Ossur "Power Knee" uses electromagnetic actuation, which limits the battery life.

3. Motivation and Contribution

One of the most significant challenges in the development of a powered lower limb prosthesis is providing self-powered actuation capabilities comparable to biological systems. State-of-the-art power supply and actuation technology such as battery/DC motor combinations suffer from low energy density of the power source (i.e., heavy batteries for a given amount of energy), low actuator force/torque density, and low actuator power density (i.e., heavy motor/gearhead packages for a given amount of force or torque and power output), all relative to the human musculoskeletal system. Recent advances in power supply and actuation for self-powered robots, such as the liquid-fueled approaches described by Goldfarb et al. 2003, Shields et al. 2006, Fite et al. 2006, and Fite and Goldfarb 2006, offer the potential of significantly improved energetic characteristics relative to battery/DC motor combinations, and thus bring the potential of a powered lower limb prosthesis to the near horizon. Specifically, the aforementioned publications describe pneumatic-type actuators, which are powered by the reaction products of a catalytically decomposed liquid monopropellant. The proposed approach has been experimentally shown to provide an energetic figure of merit an order of magnitude greater than state-of-the-art batteries and motors (Shields et al. 2006, Fite and Goldfarb 2006). Based on this liquid-fueled approach, a prototype of a powered knee and ankle transfemoral prosthesis have been developed (Sup and Goldfarb 2007).

The development of a powered prosthesis changes significantly the nature of the user-prosthesis interface and control problem. Unlike a passive device (e.g., a modulated damper knee joint) that can fundamentally only react to a user’s input, a powered device can both act as well as react. As such, the prosthesis necessitates a reliable control framework for generating required joint torques while ensuring stable and coordinated interaction with the user and the environment. This thesis proposes an intelligent control framework for the control of the powered knee and ankle transfemoral prosthesis.

4. Organization of the Document

The thesis is organized into four chapters. The references for each chapter is given at the end of the chapter. Chapter I presents the introduction and motivation for the intelligent control of a powered transfemoral prosthesis. Chapter II is a conference paper that is published in the Proceedings of the *10th International Conference on Rehabilitation Robotics (ICORR 2007)*. The paper presents a k-Nearest Neighbor algorithm based real-time gait intent recognition approach for use in controlling a fully powered transfemoral prosthesis described. The proposed approach infers user intent based on the characteristic shape of the force and moment vector of interaction between the user and prosthesis.

Chapter III is also a conference paper that is published in the Proceedings of the *10th International Conference on Rehabilitation Robotics (ICORR 2007)*. This paper presents an active passive torque decomposition procedure for use in controlling a fully powered transfemoral prosthesis. The active and passive parts of the joint torques are extracted by solving a constrained least squares optimization problem. The proposed approach generates the torque reference of joints by combining the active part, which is a function of the force and moment vector of the interaction between user and prosthesis and the passive part, which has a nonlinear spring-dashpot behavior. The last chapter, Chapter IV, describes the experimental procedure for the calibration of the three axis socket load cell, the main component of the mechanical sensory interface of the powered prosthesis.

5. References

Au, S. Bonato, P., Herr, H., “An EMG-Postion Controlled System for an Active Ankle-Foot Prothesis: An Initial Experimental Study,” Proceedings of the IEEE Int Conf. on Rehabilitation Robotics, pp. 375-379, 2005.

DeVita, P., Torry M., Glover, K.L., and Speroni, D.L.,“A Functional Knee Brace Alters Joint Torque and Power Patterns during Walking and Running,” Journal of Biomechanics, vol. 29, no. 5, pp. 583-588, 1996.

Donath, M., “Proportional EMG Control for Above-Knee Prosthesis’, Department of Mechanical Engineering Masters Thesis, MIT, 1974.

Fite, K.B., and Goldfarb, M. Design and Energetic Characterization of a Proportional-Injector Monopropellant-Powered Actuator, IEEE/ASME Transactions on Mechatronics, vol. 11, no. 2, pp. 196-204, 2006.

Fite, K.B., Mitchell, J., Barth, E.J., and Goldfarb, M. A Unified Force Controller for a Proportional-Injector Direct-Injection Monopropellant-Powered Actuator, ASME Journal of Dynamic Systems, Measurement and Control, vol. 128, no. 1, pp. 159-164, 2006.

Flowers, W.C., “A Man-Interactive Simulator System for Above-Knee Prosthetics Studies, Department of Mechanical Engineering PhD Thesis, MIT, 1973.

Flowers, W.C., and Mann, R.W., “Electrohydraulic knee-torque controller for a prosthesis simulator,” ASME Journal of Biomechanical Engineering, vol. 99, no. 4, pp. 3-8., 1977.

Goldfarb, M., Barth, E.J., Gogola, M.A. and Wehrmeyer, J.A., “Design and Energetic Characterization of a Liquid-Propellant-Powered Actuator for Self-Powered Robots.,” IEEE/ASME Transactions on Mechatronics, vol. 8, no. 2, pp. 254-262, 2003.

Grimes, D. L., “An Active Multi-Mode Above Knee Prosthesis Controller. Department of Mechanical Engineering PhD Thesis, MIT., 1979.

Grimes, D. L., Flowers, W. C., and Donath, M., “Feasibility of an active control scheme for above knee prostheses. ASME Journal of Biomechanical Engineering, vol. 99, no. 4, pp. 215-221, 1977.

Jacobs, R., Bobbert, M.F., van Ingen Schenau, G.J.; “Mechanical output from individual muscles during explosive leg extensions: the role of biarticular muscles,” Journal of Biomechanics, vol. 29, no. 4, pp. 513-523, 1996.

Klute, G.K., Czerniecki, J., Hannaford, B., “Development of Powered Prosthetic Lower Limb, Proceedings of the First National Meeting, Veterans Affairs Rehabilitation Research and Development Service, 1998.

Klute, G.K., Czerniecki, J., Hannaford, B., “Muscle-Like Pneumatic Actuators for Below-Knee Prostheses, Proceedings the Seventh International Conference on New Actuators, pp. 289-292, 2000.

Nadeau, S., McFadyen, B.J., and Malouin, F., “Frontal and sagittal plane analyses of the stair climbing task in healthy adults aged over 40 years: What are the challenges compared to level walking?,” Clinical Biomechanics, vol. 18, no. 10, pp. 950-959., 2003.

Nagano, A., Ishige, Y., and Fukashiro, S., “Comparison of new approaches to estimate mechanical output of individual joints in vertical jumps,” Journal of Biomechanics, vol. 31, no. 10, pp. 951-955, 1998.

Popovic, D. and Schwirtlich, L., “Belgrade active A/K prosthesis, “ in de Vries, J. (Ed.), Electrophysiological Kinesiology, Interm. Congress Ser. No. 804, Excerpta Medica, Amsterdam, The Netherlands, pp. 337–343, 1988.

Popovic D, Oguztoreli MN, Stein RB., “Optimal control for an above-knee prosthesis with two degrees of freedom,” Journal of Biomechanics, vol. 28, no. 1, pp. 89-98, 1995.

Prilutsky, B.I., Petrova, L.N., and Raitsin, L.M., “Comparison of mechanical energy expenditure of joint moments and muscle forces during human locomotion,” Journal of Biomechanics, vol. 29, no. 4, pp. 405-415, 1996.

Riener, R., Rabuffetti, M., and Frigo, C., “Joint powers in stair climbing at different slopes.”, Proceedings of the IEEE International Conference on Engineering in Medicine and Biology, vol. 1, p. 530., 1999.

Shields, B.L., Fite, K., and Goldfarb, M. Design, Control, and Energetic Characterization of a Solenoid Injected Monopropellant Powered Actuator, IEEE/ASME Transactions on Mechatronics, vol. 11, no. 4, pp. 477-487, 2006.

Stein, J.L., “Design Issues in the Stance Phase Control of Above-Knee Prostheses,” Department of Mechanical Engineering PhD Thesis, MIT, 1983.

Stein, J.L., and Flowers, W.C., “Stance phase control of above-knee prostheses: knee control versus SACH foot design,” Journal of Biomechanics, vol. 20, no. 1, pp. 19-28, 1988.

Sup, F., Amit, B., and Goldfarb M., "Design and Control of a Powered Knee and Ankle Prosthesis," Proceedings of the 2007 IEEE International Conference on Robotics and Automation, pp. 4134-4139.

Waters, R., Perry, J., Antonelli, D., and Hislop, H., “Energy cost of walking amputees: the influence of level of amputation,” J. Bone and Joint Surgery. 58A, 42–46, 1976.

Winter, D. A. and Sienko, S. E., “Biomechanics of below-knee amputee gait,” J. Biomechanics. 21, 361–367., 1988.

Winter, D.A., “The biomechanics and motor control of human gait: normal, elderly and pathological,” University of Waterloo Press, 2nd ed., 1991.

CHAPTER II

MANUSCRIPT I: REAL-TIME INTENT RECOGNITION FOR A POWERED KNEE AND ANKLE TRANSFEMORAL PROSTHESIS

Huseyin Atakan Varol and Michael Goldfarb

Department of Mechanical Engineering

Vanderbilt University

Nashville, TN 37235

ICORR 2007 10th International Conference on Rehabilitation Robotics

June 13-15, 2007, Noordwijk, Netherlands

1. Abstract

This paper describes a real-time gait intent recognition approach for use in controlling a fully powered transfemoral prosthesis. Rather than utilize an “echo control” approach as proposed by others, which requires instrumentation of the sound-side leg, the proposed approach infers user intent based on the characteristic shape of the force and moment vector of interaction between the user and prosthesis. The real-time intent recognition approach utilizes a K-nearest neighbor algorithm with majority voting and threshold biasing schemes to increase its robustness. The ability of the approach to recognize in real time a person’s intent to stand or walk at one of three different speeds is demonstrated on measured biomechanics data.

2. Introduction

Despite significant technological advances over the past decade, such as the introduction of microcomputer-modulated damping during swing, commercial transfemoral prostheses remain essentially limited to energetically passive devices. That is, the joints of the prostheses can either store or dissipate energy, but cannot provide net power over a gait cycle. The knee and ankle joints of the native limb, however, generate significant net power output over a gait cycle during many locomotive functions, including walking upstairs and up slopes, running, and jumping (Winter and Sienko 1988, Nadeau et al. 2003, Riener et al. 1999, Prilutsky et al. 1996, DeVita et al. 1996, Nagano et al. 1998, Jacobs et al. 1996) . Even during level walking, transfemoral amputees with passive prostheses exhibit asymmetric gait kinematics, expend up to 60% more metabolic energy relative to healthy subjects (Walters et al. 1976), and exert as much as three times the affected-side hip power and torque relative to healthy subjects, all of which are indicative of the functional limitations of passive joints (Winter 1991).

A major reason for the absence of powered joints in transfemoral (and transtibial) prostheses is the lack of energy source and actuator with suitable power density to provide the power and energy required for gait in a low-weight device. Recent advances in power supply and actuation for self-powered robots, such as the liquid-fueled approach developed by Goldfarb et al. (Goldfarb et al. 2003, Shields et al. 2006, Fite et al. 2006, Fite and Goldfarb 2006), offer a power density that makes feasible a powered lower limb prosthesis. Based on this liquid-fueled approach, the authors have developed a prototype of a powered knee and ankle transfemoral prosthesis, as shown in Figure 2-1 (Sup and Goldfarb, 2006). The development of a powered prosthesis changes significantly the nature of the user-prosthesis interface and control problem. Unlike a passive device (e.g., a modulated damper knee joint) that can fundamentally only react to a user's input, a powered device can both act as well as react. As such, the prosthesis necessitates a reliable control framework for generating required joint torques while ensuring stable and coordinated interaction with the user and the environment.

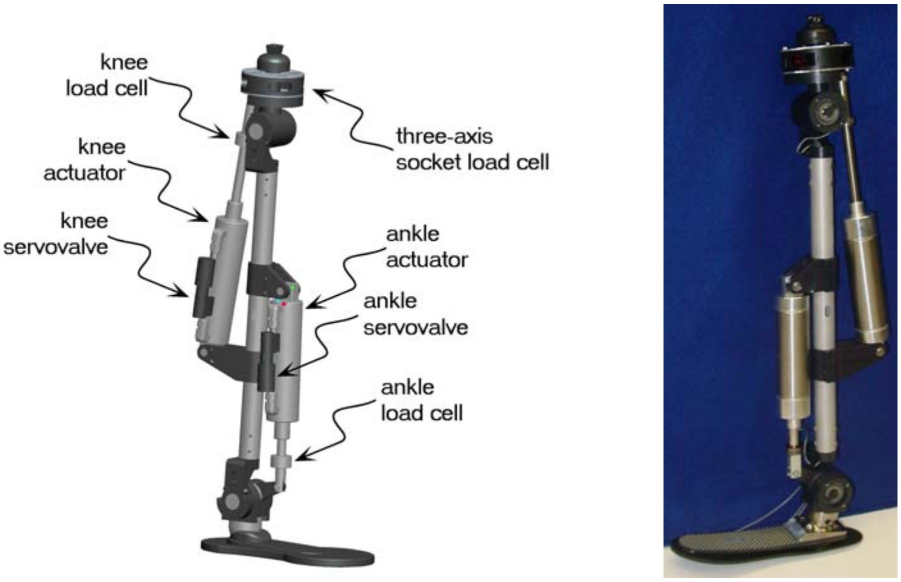

Figure 2-1. Power knee and ankle prosthesis prototype.

3. Prior Work in Powered Transfemoral Prosthesis

The authors are not aware of any prior work in the development of a powered knee and ankle transfemoral prosthesis, although prior work has been published in the development of powered knee transfemoral prostheses. Specifically, Flowers et al. developed a tethered electrohydraulic transfemoral prosthesis that consisted of a hydraulically actuated knee joint tethered to a hydraulic power source and off-board electronics and computation (Flowers et al. 1973, Donath et al. 1974, Grimes et al. 1979, Grimes et al. 1977, Stein et al. 1983, Flowers et al. 1977). They subsequently developed an "echo control" scheme for gait control, as described by Grimes et al. (1977), in which a modified knee trajectory from the sound leg is played back on the contralateral side. Popovic and Schwirtlich (1988) report the development of a battery-powered active knee joint actuated by DC motors, together with a finite state knee controller that utilizes robust position tracking control algorithm for gait control. Finally, Ossur, a major prosthetics company based in Iceland, has announced the limited launch of a powered knee, called the "Power Knee," which purportedly uses sensors on the sound side leg as input for the control of the powered prosthesis.

4. Interface Approaches

Unlike existing passive prostheses (including microprocessor-controlled devices), the introduction of power into a prosthesis provides the ability for the device to act, rather than simply react. As such, the development of a suitable controller that provides for stable and reliable interaction between the user and prosthesis is paramount. The user interface and control issue can be addressed with widely varying approaches and at widely varying degrees of invasiveness. The major categories of interface, in order of increasing invasiveness, are (1) mechanical sensory interface, (2) surface electromyography (EMG) interface, (3) implantable peripheral nervous systems (PNS) interface, and (4) implantable central nervous system (CNS) interface. Mechanical sensory interface (MSI) approaches use only sensors pertaining to the biomechanics of gait (i.e., as opposed to the physiology of gait), such as measurement of forces, torques, joint angles, and vertical orientation (i.e., inclination). Surface EMG, which is the approach used by actively powered myoelectric upper extremity prostheses, incorporates surface electrodes (often in the prosthesis socket) to extract command signals from the muscles in the residual limb. Some researchers have investigated the use of surface EMG control approaches for knee control in a lower limb prostheses, including (Aeyels et al. 1995, Donath 1974, Myers and Moskowitz 1981, Myers and Moskowitz 1983, Triolo and Moskowitz 1982, Aeyels et al. 1992, Peeraer et al. 1990). In the case of an upper extremity above-elbow myoelectric prosthesis, the combination of the biceps and triceps EMG provides a single bipolar signal, which is switched between the control of the terminal device and control of the elbow (i.e., does not enable simultaneous control of both joints). This approach would not be appropriate for an active knee and ankle joint leg, however, since locomotion requires simultaneous control of the knee and ankle. As such, an EMG approach would require at least two control channels (i.e., measurement from two sets of antagonist muscles). Implantable PNS approaches include the use of percutaneous electrodes implanted in the nerves, and/or the use of implantable capsules for extraction of the EMG signals, from which neural or EMG commands can be extracted. Finally, implantable CNS approaches utilize electrode arrays implanted in the cortex of the brain, from which motor commands can also be extracted. Presumably, the extent of control over the prosthesis would vary roughly inversely with the extent of invasiveness.

As with any medical device or procedure, one would optimally wish to incorporate the least invasive approach that achieves the desired specific aims, and as such, the proposed controller utilizes the non-invasive mechanical sensory interface approach. The lower limb, in particular, lends itself much more readily to non-invasive interface approaches than does the upper limb, since (1) the lower limb fundamentally interacts mechanically with the environment (i.e., the ground and the user) and (2) the tasks in which the lower limb engages are typically periodic in nature. Both of these qualities are leveraged in the proposed design.

Although the commercially available passive computer controlled knee systems (e.g., C-leg, Rheo knee) already make use of signals only taken from the instrumented prosthesis for real-time mode detection and subsequent knee control, the previously cited works on powered knees all incorporate a variation of echo control, in which the sound-side (i.e., unaffected) leg is instrumented to provide input commands for the powered prosthesis. The obvious drawback to such an approach is that the sound-side (or unaffected) leg must be instrumented, which requires the user to don and doff additional equipment and associated wiring. The echo control approach also restricts the use of the prosthesis to unilateral amputees and also presents a problem for “odd” numbers of steps, in which an echoed step is undesirable. A more subtle, although perhaps more significant shortcoming of the echo-type approach is that suitable motion tracking requires a high output impedance of the prosthesis, which forces the amputee to react to the limb rather than interact with it. Specifically, in order for the prosthesis to dictate the joint trajectory, it must assume a high output impedance (i.e., must be stiff), thus precluding any dynamic interaction with the user and the environment, which is in turn contrary to the way in which humans interact with their native limbs.

This paper offers an alternative approach to addressing the interface between user and prosthesis that is both non-invasive and obviates the need for sound-side instrumentation. Rather than gather user intent from the joint angle measurements from the contralateral unaffected leg, the proposed approach infers commands from the user via the (ipsilateral) forces and moments of interaction between the user and prosthesis. Specifically, the user interacts with the prosthesis by imparting forces and moments from the residual limb to the prosthesis, all of which can be measured via a multi-axis load cell. These forces and moments serve not only as a means of physical interaction, but also serve as an implicit communication channel between the user and device, with the user's intent encoded in this measurement. Inferring user's intent from the measured forces and moments of interaction provides several advantages relative to the echo approach. First, no instrumentation or wiring apart from the prosthesis need be worn by the user. Second, unlike an echo approach, the information flow is immediate (i.e., the user intent need not be delayed by a half cycle). Third, the prosthesis command is decoupled from the unaffected side, and thus the user is not constrained to "even" patterns of gait. Finally, unlike an echo approach, the proposed approach can be utilized on either a unilateral or bilateral amputee.

This paper describes a method for the real-time recognition of user intent based primarily on the forces and moments of interaction between the user and prosthesis, and demonstrates on biomechanical data that the proposed approach can differentiate between standing and three different walking speeds.

5. K-Nearest Neighbor Classification

Gait intent recognition is a real time pattern recognition or signal classification problem. The signal in this case is the combination of socket interface forces and the dynamic state of the prosthesis, which is a vector of the knee and ankle angles as illustrated in Figure 2-2. Many methods exist for pattern recognition and signal classification including nearest neighbor algorithms, neural networks, fuzzy classifiers, linear discriminant analysis, and genetic algorithms (Duda et al. 2001). Though each has its respective virtues, a k-nearest neighbor (k-NN) approach provides the advantages of relatively little training information and minimal computation, both of which render it particularly appropriate for real-time applications with limited computational capacity, such as the one proposed.

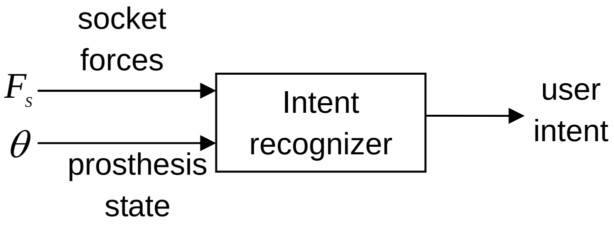

Figure 2-2. Structure of the transfemoral prosthesis control system..

5.1 K-Nearest Neighbor Algorithm

First proposed by Fix and Hodges (1951), the nearest neighbor rule is one of the simplest pattern classification algorithms. The approach classifies unlabeled examples based on their similarity with examples in the training set. Given a set of n labeled subsets, $D_n = \{(X_1, Y_1), (X_2, Y_2), \ldots, (X_n, Y_n)\}$, where X_i are the feature vectors in some input space and $Y_i \in \{w_1, w_2, \ldots, w_n\}$ are the corresponding class labels, the k-nearest neighbor rule finds the k "closest" labeled examples in the training set and classifies x_u into the class that appears most frequently within the k-subset.

The approach is most easily illustrated by the example shown in Figure 2-3, in which we wish to classify the unknown data point, x_u, into one of four classes. In this case, the Euclidian distance metric is chosen to quantify the "closeness," and the number of the nearest neighbors (k) to which we would like to quantify the closeness of the data point is chosen to be five (note that the number depends on the number of classes, number of points, nature of the classes, etc.). As depicted in the figure, three of the nearest neighbors belong to the class w_4, while two belong to the class w_1. The data point is therefore assigned to class w_4, since it has the most "nearest neighbors" in that class.

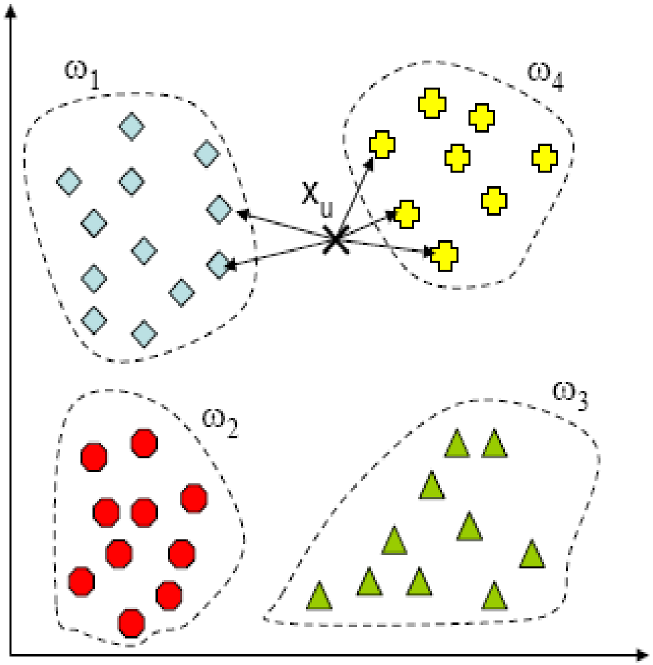

Figure 2-3. Illustration of the k-NN algorithm for the classification of an unknown example, x_u, with 5 nearest neighbors and 4 classes.

5.2 Application of k-NN to Gait Mode Recognition

For purposes of intent recognition in a powered prosthesis, the algorithm must be fast (relative to the step period), must be real-time (i.e., satisfaction of hard deadline constraints is needed due to the safety critical nature of the task), must be robust to noise, and must be computationally inexpensive since it will be implemented on an embedded computing platform with limited computational capability.

In this work, the k-NN algorithm described in the previous section is modified and enhanced to detect the different gait modes. At this point in its development, the k-NN based intent recognizer detects four different gait modes, q_i, which are standing (q_1) and three different walking speeds (slow (q_2), normal (q_3) and fast (q_4)). Note that in a realistic implementation, several classes would be considered, including walking upstairs and downstairs and walking backwards. Despite this, the aforementioned set of four classes serves as an appropriate initial set with which to develop and test the proposed approach.

At each time step of the algorithm, an unlabeled example vector consisting of the sensor measurement vector, $x_u = [F_{S_1}, F_{S_2}, \theta_{knee}, \theta_{ankle}]^T$, is classified as one of the four gait modes. The sensor measurement consists of the socket load forces in the sagittal plane, F_{S_1} and F_{S_2}, and the knee and ankle angles, θ_{knee} and θ_{ankle}. At each iteration, the distance of the new unclassified sample relative to the each class of data points is calculated. Two measures of closeness were compared, the Euclidian norm and the absolute norm. The distance of the unclassified sample vector, x_u, relative to a vector, x_i, in the training set is given for the Euclidian and absolute case respectively as:

$$c_{i_{euclidian}} = \sqrt{\sum_{j=1}^{4} (x_{u_j} - x_{i_j})^2} \qquad (1)$$

$$c_{i_{abs}} = \sum_{j=1}^{4} \left| x_{u_j} - x_{i_j} \right| \qquad (2)$$

Once the k nearest neighbors are determined, the sample vector is classified as the class with the most members of this set. In order to decrease sensitivity to noise, classification of the current sample vector is additionally debounced and filtered. The debouncing is based on a threshold biasing scheme, in which at each time step, the number of members of the nearest neighbor set for the predominant class in the previous time step is multiplied by a biasing constant, $a > 1$. Appropriate tuning of this parameter decreases the likelihood of switching classes, and thus inhibits chattering between classes. The output of the classifier is additionally filtered by a boxcar window of length p. Figure 2-4 lists the psuedocode of the classification algorithm.

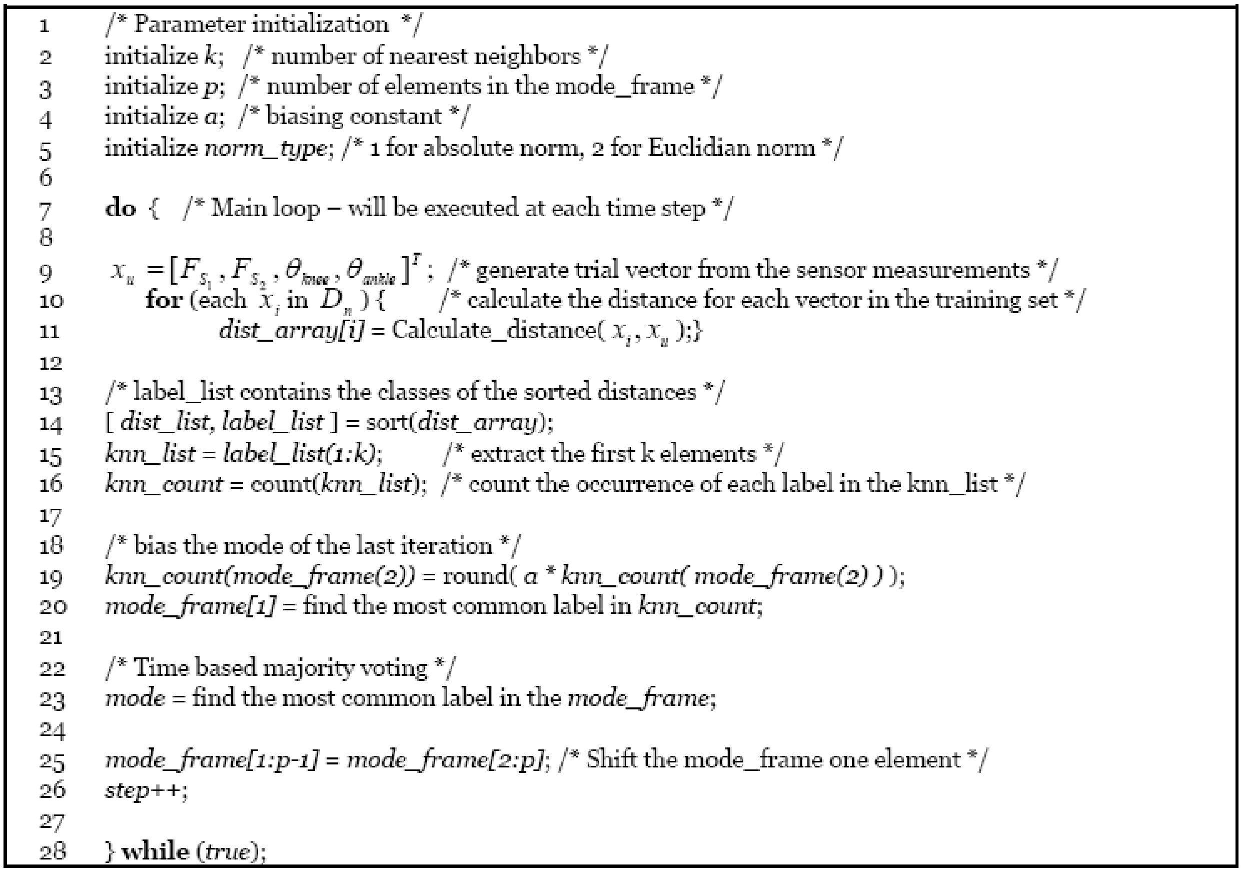

```
/* Parameter initialization */
initialize k; /* number of nearest neighbors */
initialize p; /* number of elements in the mode_frame */
initialize a; /* biasing constant */
initialize norm_type; /* 1 for absolute norm, 2 for Euclidian norm */

do { /* Main loop – will be executed at each time step */

 $x_u = [F_{S_1}, F_{S_2}, \theta_{knee}, \theta_{ankle}]^T$; /* generate trial vector from the sensor measurements */
    for (each $x_i$ in $D_n$) {     /* calculate the distance for each vector in the training set */
            dist_array[i] = Calculate_distance( $x_i$, $x_u$ );}

/* label_list contains the classes of the sorted distances */
[ dist_list, label_list ] = sort(dist_array);
knn_list = label_list(1:k);        /* extract the first k elements */
knn_count = count(knn_list); /* count the occurrence of each label in the knn_list */

/* bias the mode of the last iteration */
knn_count(mode_frame(2)) = round( a * knn_count( mode_frame(2) ) );
mode_frame[1] = find the most common label in knn_count;

/* Time based majority voting */
mode = find the most common label in the mode_frame;

mode_frame[1:p-1] = mode_frame[2:p]; /* Shift the mode_frame one element */
step++;

} while (true);
```

Figure 2-4. Pseudocode of the k-NN based intent recognition algorithm.

6. Implementation and Experimental Validation

6.1 Gait Experiments

In order to validate the ability of the proposed approach to determine user intent in real-time, the authors generated an experimental database consisting of the appropriate data vectors for various data classes (i.e., for standing and three different walking speeds). Note that two major differences exist between the conditions used for validation of the approach and the manner in which the approach would eventually be implemented in a prosthesis. First, the gait data was generated by a normal subject rather than from an amputee. Second, the intent recognition algorithm was tested following the collection of all data, rather than in a real-time setting. Both variations were a matter of experimental convenience, and neither affects significantly the validity of the results. Specifically, the use of a normal subject rather than an amputee affects two issues. First, the mass distribution of the leg will be slightly different than if it were a prosthesis. Second, since the vector of sagittal plane forces of interaction between the user and prosthesis is not readily measured in a normal subject, the algorithm instead used the vector of sagittal plane hip torque and ground reaction force, which are related to the former by a coordinate transformation. In other words, both force vectors fundamentally contain the same information, but are simply measured in different locations. Regarding the real-time aspect, the algorithm was required to run at a high sampling speed (i.e., 10 msec) and to be strictly causal, and as such could have been implemented in real-time. Due to the use of a normal subject, however, the real-time implementation was not possible, since the hip torque could not be directly measured, but rather had to be computed via post-processing of the measured data (as is typical in the acquisition of kinetic gait data). Note that in a transfemoral prosthesis (such as the one shown in Figure 2-1), the force data would be measured on the prosthesis, and thus would be available for real-time use.

In order to generate appropriate kinematic and kinetic data for definition of the data classes and for testing of the approach, gait experiments were conducted in the Biomechanics and Sports Medicine Laboratory of the University of Tennessee at Knoxville. The experimental setup consisted of a 7-camera 240 Hz VICON MX system and 2 AMTI multiaxis force platforms. As is standard in such a setup, hip, knee and ankle angles were measured via the cameras, the ground reaction force was measured using the multiaxis force plates, and the joint torques and forces were computed in post-processing via inverse dynamics, based on inertial parameters estimated with lookup tables. The sampling rate for the cameras and the force plates were 100 Hz and 1000 Hz, respectively. Data collection consisted of two 30-second trials for standing (ST) and four trials each for standing to walking (S2W), walking to standing (W2S), slow walking (WS), normal walking (WN) and fast walking (WF). In the standing trials, the subject was asked to stand and shift his weight around as he normally would. For the stand to walk transition, the subject was asked to stand on the force plate for approximately five seconds, then proceed to a normal walk at a self-selected pace. For the walk to stand transition, the subject was asked to walk at a self-selected pace, then as naturally as possible come to a stop on the force plate. For the slow, normal, and fast walking, the subject was asked to walk at those respective rates, while an optical interrupt timing system measured the walking speed between the subject's entrance and exit of the camera viewing volume. The minimum, maximum and average speeds for each class of walking speeds are shown in Table 2-1. The experimental setup and the human subject are shown during a measurement trial in Figure 2-5.

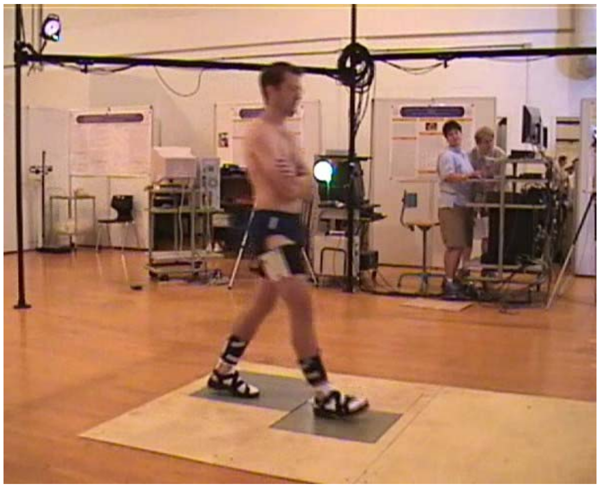

Figure 2-5. Data collection for the demonstration of the proposed approach.

6.2 Class Database and Generation of Test Sequences

Since kinetic data is only available during contact with the force plates, the amount of data with which to define various classes and test the system was limited. Given the limited amount of data, all trials of each class were concatenated to form the database defining that particular class (i.e., standing, slow walking, normal walking, and fast walking). The “test” data was formed by assembling linear combinations of trial data and by inserting stand to walk and walk to stand transition data between the standing and walking data. Then the test data is smoothed with a low pass filter in order to remove the spikes occurring due to the concenation of the datasets. Recall, that each training set contains time marked arrays of the hip torque, the ground reaction force, knee and ankle angles, all at a sampling rate of 10 ms. The components of each data set were additionally scale-normalized between 0 and 1 in order to make the relative importance of all the time marked arrays equal. Note that the normalization constants obtained from the training data will also be employed to normalize the measurement data at each sampling instant in the real-time application. Note also that the objective of the intent recognizer is only to determine intent for a single user, as opposed to generalized intent recognition across subjects. As such, each subject would require a separate database defining the various classes of locomotion (i.e., a database representing the spectrum of user intentions).

TABLE 2-1

WALKING EXPERIMENT PARAMETERS

Walking Mode	Minimum Speed (m/s)	Average Speed (m/s)	Maximum Speed (m/s)
Slow	1.01	1.04	1.07
Normal	1.19	1.22	1.26
Fast	1.45	1.51	1.56

Figure 2-6 shows an example of a "test" sequence of data, which represents a walking trial containing several different modes of gait over a total duration of approximately 25 seconds. In the trial scenario, the standing experimental subject starts with a transition from standing to slow walking, and then accelerates to normal and subsequently to fast walking. After two strides of fast walking, the person decelerates to normal and then slow walking. At the end of the trial, a transition from slow walking to standing is performed.

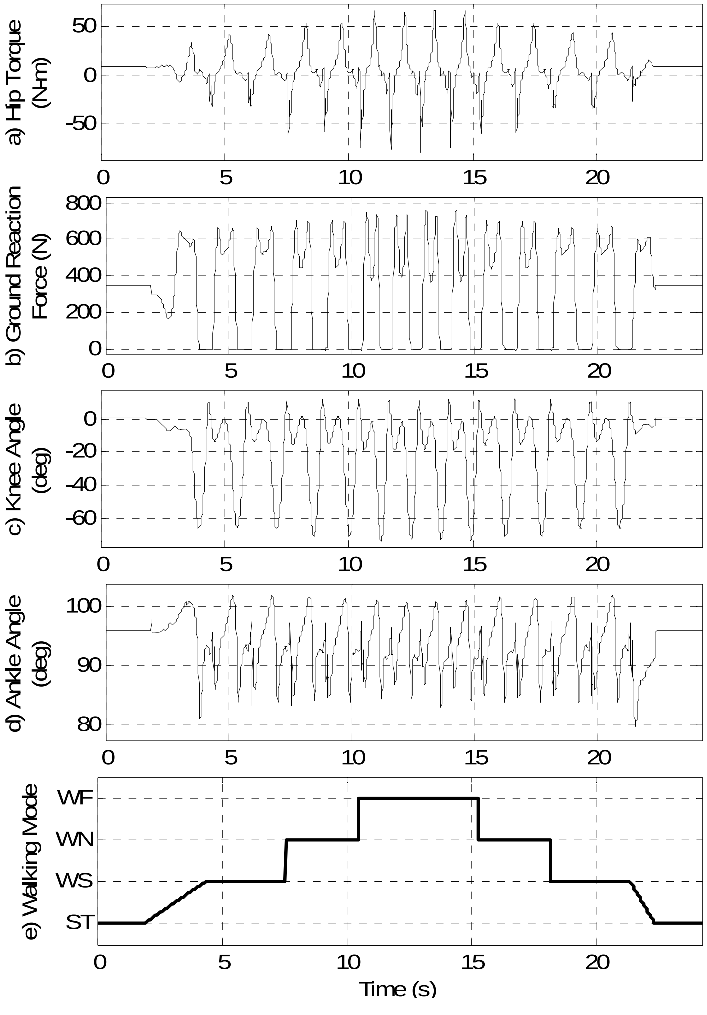

Figure 2-6. The hip torque (a), the ground reaction force (b), the knee angle (c), the ankle angle (d), and the different walking modes (e) for an example walking trial scenario.

7. Results and Discussion

The k-NN intent recognizer was implemented on a PC with an Intel Pentium 4 (2 GHz) processor with 1024MB memory using Matlab 7.0. In order to simulate real-time conditions, the algorithm was run with a fixed time step of 10 msec. The algorithm includes three parameters which can be tuned, based on the nature and amount of noise in the data, to result in the least mode estimation error. The three parameters are the biasing constant, a, the number of nearest neighbors, k, and the length of the boxcar window, p. The value of the biasing constant, a, was experimentally tuned independently of the other parameters. A higher value of this constant makes the algorithm more robust and prevents chattering between different modes, but, it also causes delays in the transitions which is not desirable. Figure 2-7 shows a trial scenario depicting a transition from normal walking to fast walking. As can be seen, when the parameter $a = 2$, the transition is recognized in approximately 0.17 seconds, although chattering is present in the classification. In the case that $a = 3$, the chattering does not occur and the delay in the recognition is nearly the same. When $a = 4$, the transition delay increases substantially to 0.4 seconds. As such, the biasing constant was set to $a = 3$ for the work presented here, which was determined to be the best trade-off between delay and chatter.

For the data shown in Figure 2-6, the values of the other two parameters were determined by an exhaustive search for the smallest estimation error with integer values of the parameters $3 \le k \le 25$ and $2 \le p \le 32$. The results of this search for both absolute and the Euclidian norms are shown in Table 2-2, which indicates that the smallest mode identification error is obtained when the absolute norm is used and the values of nearest neighbors, k, and the length of the boxcar window, p, are set to 7 and 16 respectively. The results for the “best case” set of parameters are therefore $a = 3$, $k = 7$, and $p = 16$, with the best distance metric being the absolute norm. Using these parameters on a different sequence of walking data, Figure 2-8 shows the intent recognition results for the three cases consisting of (a) the unmodified k-NN algorithm, (b) the k-NN algorithm with biasing constant, and (c) the k-NN algorithm with biasing and filtering. It can be easily seen that the biasing constant and filtering schemes improve the performance.

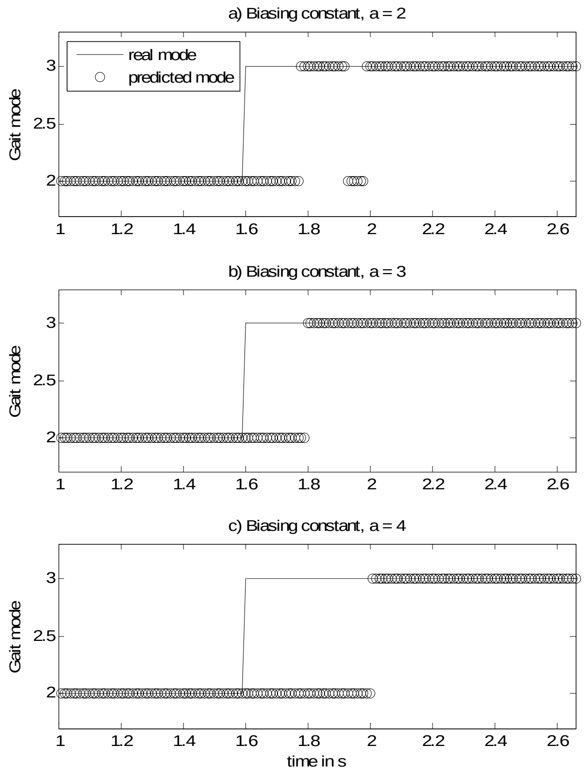

Figure 2-7. Effect of biasing constant on chattering and delay.

TABLE 2-2
MODE IDENTIFICATION ERROR FOR DIFFERENT PARAMETERS (%)
(ABSOLUTE NORM (LEFT), EUCLIDIAN NORM (RIGHT))

	p=2	p=4	p=8	p=16	p=32
k=3	6.53/7.88	5.91/7.51	4.85/6.02	3.07/5.06	3.41/5.54
k=5	5.48/6.99	5.24/6.84	4.37/5.46	3.17/4.57	3.27/3.98
k=7	4.23/4.98	3.94/4.68	4.08/4.91	**2.69/**4.31	3.41/5.46
k=11	3.65/6.28	3.7/6.13	3.89/5.91	3.65/5.84	4.13/5.76
k=15	4.03/4.39	4.27/4.65	4.61/4.8	4.71/5.24	4.95/5.5
k=25	5.19/6.13	5.38/6.36	5.38/6.58	5.57/7.14	6.68/7.32

The value of the parameter, a, is set to 3 in all the cases.

Regarding real-time implementation, the computation time for the case shown in Figure 2-8(c) was approximately 10% of the real-time (i.e., in real time, the algorithm would require approximately 10% of the processor utilization). It should be noted that the code execution time could be decreased by converting the code to a compiled language such as C++, although it should also be noted that an increased number of possible gait modes would increase code execution time.

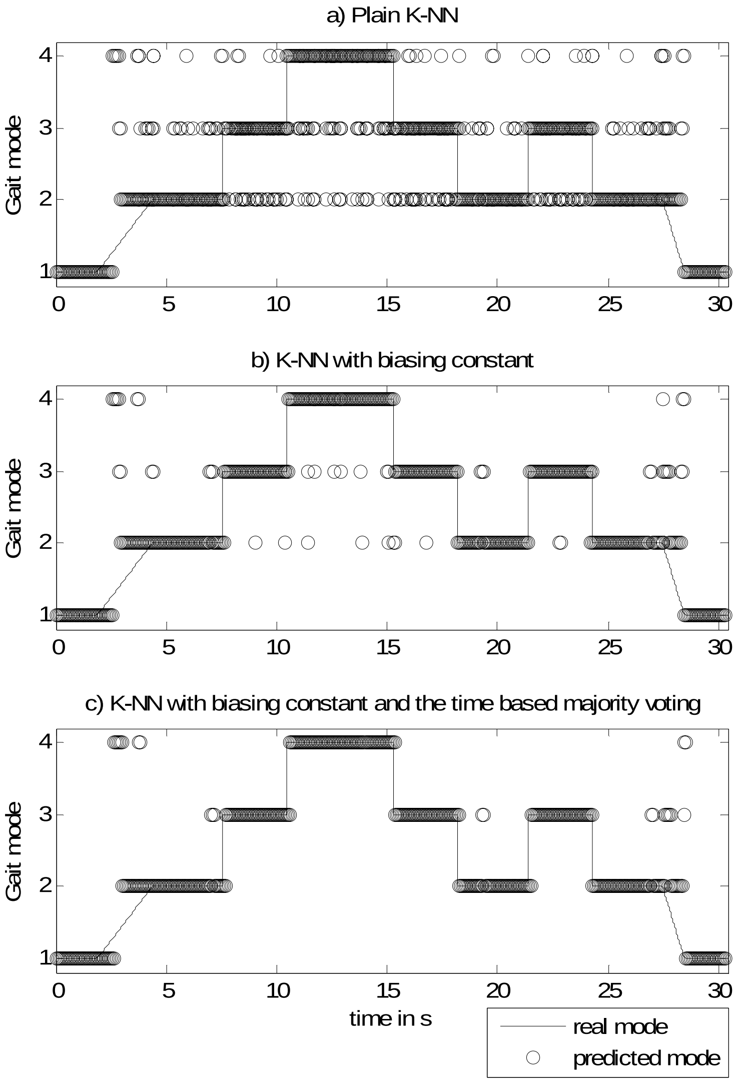

Figure 2-8. Mode estimation for a 30.42 seconds trial walking scenario with the (a) plain k-NN algorithm, (b) k-NN with the biasing constant, (c) k-NN with both the biasing constant and the time based majority voting.

8. Conclusion

The authors hypothesized that a user’s intent could be reliably inferred in real-time based on pattern recognition of the measured forces and moments of interaction between the user and prosthesis. Based on a proposed k-NN intent recognizer and biomechanical experiments designed to validate the proposed approach, the notion of extracting in real-time user’s intent from socket interaction forces appears highly feasible. Further work includes testing the ability to extract user intent for other gait modes, including stair ascent/descent, slope ascent/descent, and backward walking. Further work additionally includes testing the proposed intent recognition approach on transfemoral amputees in a real-time setting.

9. References

Aeyels, B., Peeraer, L., Vander Sloten, J., Van der Perre, G., Development of an above-knee prosthesis equipped with a microcomputer-controlled knee joint: first test results. Journal of Biomedical Engineering, Vol. 14, pp. 199-202, 1992.

Aeyels, B., Van Petegem, W., Vander Sloten, J., Van der Perre, G. and Peeraer, L., EMG-based finite state approach for a microcomputer-controlled above-knee prosthesis, Annual International Conference of the IEEE Engineering in Medicine and Biology, Proceedings of IEEE Engineering in Medicine and Biology, 1995.

DeVita, P., Torry M., Glover, K.L., and Speroni, D.L. A Functional Knee Brace Alters Joint Torque and Power Patterns during Walking and Running, Journal of Biomechanics, vol. 29, no. 5, pp. 583-588, 1996.

Donath, M., Proportional EMG Control for Above-Knee Prosthesis’, Department of Mechanical Engineering Masters Thesis, MIT, 1974.

Duda, R.O, Hart, P.E., and Stork, D.G., Pattern Classification, 2nd ed., John Wiley and Sons, 2001.

Fite, K.B., Mitchell, J., Barth, E.J., and Goldfarb, M. A Unified Force Controller for a Proportional-Injector Direct-Injection Monopropellant-Powered Actuator, ASME Journal of Dynamic Systems, Measurement and Control, vol. 128, no. 1, pp. 159-164, 2006.

Fite, K.B., and Goldfarb, M. Design and Energetic Characterization of a Proportional-Injector

Monopropellant-Powered Actuator, IEEE/ASME Transactions on Mechatronics, vol. 11, no. 2, pp. 196-204, 2006.

Fix, E. and Hodges, J. Discriminatory analysis, nonparametric discrimination: consistency properties, USAF School of Aviation Medicine, Randolph Field, Texas, Tech. Report 4, 1951.

Flowers, W.C., A Man-Interactive Simulator System for Above-Knee Prosthetics Studies, Department of Mechanical Engineering PhD Thesis, MIT, 1973.

Flowers, W.C., and Mann, R.W. Electrohydraulic knee-torque controller for a prosthesis simulator. ASME Journal of Biomechanical Engineering, vol. 99, no. 4, pp. 3-8, 1977.

Goldfarb, M., Barth, E.J., Gogola, M.A., and Wehrmeyer, J.A.. Design and Energetic Characterization of a Liquid-Propellant-Powered Actuator for Self-Powered Robots, IEEE/ASME Transactions on Mechatronics, vol. 8, no. 2, pp. 254-262, 2003.

Grimes, D. L. An Active Multi-Mode Above Knee Prosthesis Controller. Department of Mechanical Engineering PhD Thesis, MIT, 1979.

Grimes, D. L., Flowers, W. C., and Donath, M. Feasibility of an active control scheme for above knee prostheses. ASME Journal of Biomechanical Engineering, vol. 99, no. 4, pp. 215-221, 1977.

Jacobs, R., Bobbert, M.F., van Ingen Schenau, G.J. Mechanical output from individual muscles during explosive leg extensions: the role of biarticular muscles. Journal of Biomechanics, vol. 29, no. 4, pp. 513-523, 1996.

Myers, D. and Moskowitz, G., Myoelectric pattern recognition for use in the volitional control of above-knee prosthesis, IEEE Trans. Syst. Man Cybern., Vol. SMC-11 No. 4, pp. 296-302, 1981.

Myers, D. and Moskowitz, G., Active EMG-controlled A/K prosthesis. Control aspects of prosthetics and orthotics, Proceedings of the IFAC Symposium, Columbus, OH, 1983.

Nadeau, S., McFadyen, B.J., and Malouin, F. Frontal and sagittal plane analyses of the stair climbing task in healthy adults aged over 40 years: What are the challenges compared to level walking? Clinical Biomechanics, vol. 18, no. 10, pp. 950-959, 2003.

Nagano, A., Ishige, Y., and Fukashiro, S. Comparison of new approaches to estimate mechanical output of individual joints in vertical jumps. Journal of Biomechanics, vol. 31, no. 10, pp. 951-955, 1998.

Peeraer L, Aeyels B, Van der Perre G. Development of EMG-based mode and intent recognition algorithms for a computer controlled above-knee prosthesis. J. Biomed. Eng. 1990, Vol 12, 178-182.

Popovic, D. and Schwirtlich, L. Belgrade active A/K prosthesis, in de Vries, J. (Ed.), Electrophysiological Kinesiology, Intern. Congress Ser. No. 804, Excerpta Medica, Amsterdam, The Netherlands, pp.

337–343, 1988.

Prilutsky, B.I., Petrova, L.N., and Raitsin, L.M. Comparison of mechanical energy expenditure of joint moments and muscle forces during human locomotion. Journal of Biomechanics, vol. 29, no. 4, pp. 405-415, 1996.

Riener, R., Rabuffetti, M., and Frigo, C. Joint powers in stair climbing at different slopes. Proceedings of the IEEE International Conference on Engineering in Medicine and Biology, vol. 1, p. 530, 1999.

Shields, B.L., Fite, K., and Goldfarb, M. Design, Control, and Energetic Characterization of a Solenoid Injected Monopropellant Powered Actuator, IEEE/ASME Transactions on Mechatronics, vol. 11, no. 4, pp. 477-487, 2006.

Stein, J.L. Design Issues in the Stance Phase Control of Above-Knee Prostheses. Department of Mechanical Engineering PhD Thesis, MIT, 1983

Stein, J.L., and Flowers, W.C. Stance phase control of above-knee prostheses: knee control versus SACH foot design. Journal of Biomechanics, vol. 20, no. 1, pp. 19-28, 1987.

Sup, F., and Goldfarb, M. Design of a Pneumatically Actuated Transfemoral Prosthesis. Proceedings of ASME International Mechanical Engineering Conference and Exposition, IMECE2006-15707, 2006.

Triolo, R. and Moskowitz, G., Autoregressive EMG analysis and prosthetic control, Proceedings of the 35th Annual Conference on Engineering in Medicine and Biology, Philadelphia, PA, 1982.

Waters, R., Perry, J., Antonelli, D., and Hislop, H. Energy cost of walking amputees: the influence of level of amputation. J. Bone and Joint Surgery. 58A, 42–46, 1976.

Winter, D.A. The biomechanics and motor control of human gait: normal, elderly and pathological, University of Waterloo Press, 2nd ed, 1991.

Winter, D. A. and Sienko, S. E. Biomechanics of below-knee amputee gait. J. Biomech . 21, 361–367, 1988.

CHAPTER III

MANUSCRIPT II: DECOMPOSITION-BASED CONTROL FOR A POWERED KNEE AND ANKLE TRANSFEMORAL PROSTHESIS

Huseyin Atakan Varol and Michael Goldfarb

Department of Mechanical Engineering

Vanderbilt University

Nashville, TN 37235

ICORR 2007 10th International Conference on Rehabilitation Robotics

June 13-15, 2007, Noordwijk, Netherlands

1. Abstract

This paper describes an active passive torque decomposition procedure for use in controlling a fully powered transfemoral prosthesis. The active and passive parts of the joint torques are extracted by solving a constrained least squares optimization problem. Rather than utilize "echo control" as proposed by others, the proposed approach generates the torque reference of joints by combining the active part, which is a function of the force and moment vector of the interaction between user and prosthesis and the passive part, which has a nonlinear spring-dashpot behavior. The ability of the approach to reconstruct the required joint torques is demonstrated in simulation on measured biomechanics data.

2. Introduction

Despite significant technological advances over the past decade, commercial transfemoral prostheses remain essentially limited to energetically passive devices. The knee and ankle joints of the native limb, however, generate significant net power output over a gait cycle during many locomotive functions, including walking upstairs and up slopes, running, and jumping (Winter and Sienko 1988, Nadeau et al. 2003, Riener et al. 1999, Prilutsky et al. 1996, DeVita et al. 1996, Nagano et al. 1998, Jacobs et al. 1996).

A major reason for the absence of powered joints in transfemoral (and transtibial) prostheses is the lack of energy source and actuator with suitable power density to provide the power and energy required for gait in a low-weight device. Recent advances in power supply and actuation for self-powered robots, such as the liquid-fueled approach developed by Goldfarb et al. (Goldfarb et al. 2003, Shields et al. 2006, Fite et al. 2006, Fite and Goldfarb 2006), offer a power density that makes a powered lower limb prosthesis feasible. Based on this liquid-fueled approach, the authors have developed a prototype of a powered knee and ankle transfemoral prosthesis, as described in Sup and Goldfarb (2007) and shown in Figure 3-1. The development of a powered prosthesis changes significantly the nature of the user-prosthesis interface and control problem. Unlike a passive device (e.g., a modulated damper knee joint) that can fundamentally only react to a user's input, a powered device can both act as well as react. As such, the prosthesis necessitates a reliable control framework for generating required joint torques while ensuring stable and coordinated interaction with the user and the environment.

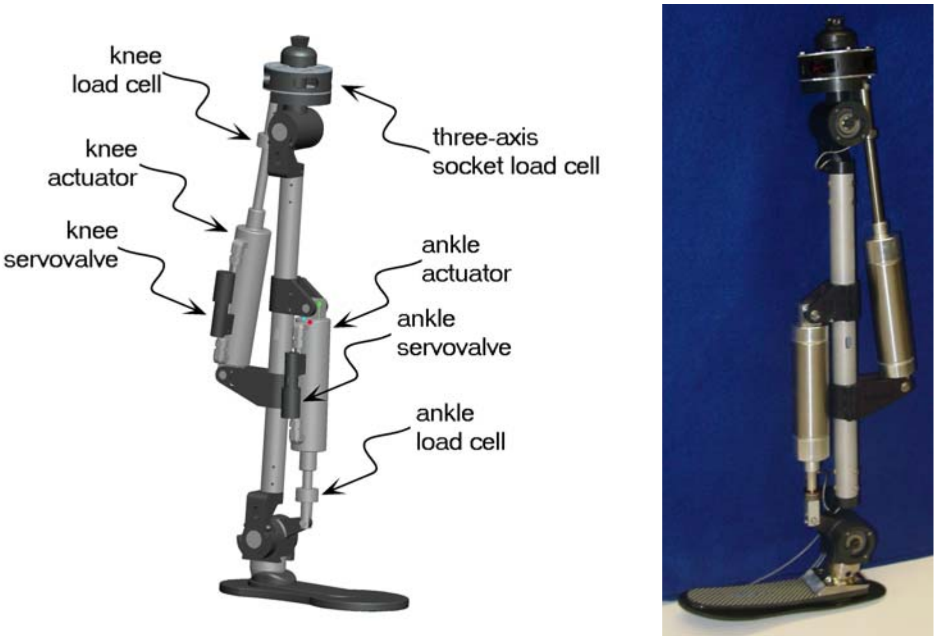

Figure 3-1. Power knee and ankle prosthesis prototype.

3. Prior Work in Powered Transfemoral Prostheses

The authors are not aware of any prior work in the development of a powered knee and ankle transfemoral prosthesis, although prior work has been published in the development of powered knee transfemoral prostheses. Specifically, Flowers et al. developed a tethered electrohydraulic transfemoral prosthesis that consisted of a hydraulically actuated knee joint tethered to a hydraulic power source and off-board electronics and computation (Flowers et al. 1973, Donath et al. 1974, Grimes 1979, Grimes et al.

1977, Stein et al. 1983, Flowers et al. 1977). They subsequently developed an “echo control” scheme for gait control, as described by Grimes et al. (1977), in which a modified knee trajectory from the sound leg is played back on the contralateral side. Popovic and Schwirtlich (1988) report the development of a battery-powered active knee joint actuated by DC motors, together with a finite state knee controller that utilizes robust position tracking control algorithm for gait control. Finally, Ossur, a major prosthetics company based in Iceland, has announced the limited launch of a powered knee, called the “Power Knee”.

4. Interface Approaches

Unlike existing passive prostheses (including microprocessor-controlled devices), the introduction of power into a prosthesis provides the ability for the device to act, rather than simply react. As such, the development of a suitable controller that provides for stable and reliable interaction between the user and prosthesis is paramount. The user interface and control issue can be addressed with widely varying approaches and at widely varying degrees of invasiveness. The major categories of interface, in order of increasing invasiveness, are (1) mechanical sensory interface, (2) surface electromyography (EMG) interface, (3) implantable peripheral nervous systems (PNS) interface, and (4) implantable central nervous system (CNS) interface. Mechanical sensory interface (MSI) approaches use only sensors pertaining to the biomechanics of gait (i.e., as opposed to the physiology of gait), such as measurement of forces, torques, joint angles, and vertical orientation (i.e., inclination). Surface EMG, which is the approach used by actively powered myoelectric upper extremity prostheses, incorporates surface electrodes (often in the prosthesis socket) to extract command signals from the muscles in the residual limb. Some researchers have investigated the use of surface EMG control approaches for knee control in a lower limb prosthesis (Aeyels et al. 1995, Donath 1974, Myers and Moskowitz 1981, Myers and Moskowitz 1983, Triolo and Moskowitz 1982, Aeyels et al. 1992, Peeraer et al. 1990). In the case of an upper extremity above-elbow myoelectric prosthesis, the combination of the biceps and triceps EMG provides a single bipolar signal, which is switched between the control of the terminal device and control of the elbow (i.e., does not enable simultaneous control of both joints). This approach would not be appropriate for an active knee and ankle joint leg, however, since locomotion requires simultaneous control of the knee and ankle. As such, an EMG approach would require at least two control channels (i.e., measurement from two sets of antagonist muscles). Implantable PNS approaches include the use of percutaneous electrodes implanted in the nerves, and/or the use of implantable capsules for extraction of the EMG signals, from which neural or EMG commands can be extracted. Finally, implantable CNS approaches utilize electrode arrays implanted in the cortex of the brain, from which motor commands can also be extracted. Presumably, the extent of control over the prosthesis would vary roughly inversely with the extent of invasiveness.

As with any medical device or procedure, one would optimally wish to incorporate the least invasive approach that achieves the desired specific aims, and as such, the proposed controller utilizes the non-invasive mechanical sensory interface approach. The lower limb, in particular, lends itself much more readily to non-invasive interface approaches than does the upper limb, since (1) the lower limb fundamentally interacts mechanically with the environment (i.e., the ground and the user) and (2) the tasks in which the lower limb engages are typically periodic in nature. Both of these qualities are leveraged in the proposed design.

The previously cited works on powered knees all incorporate a variation of echo control, in which the sound-side (i.e., unaffected) leg is instrumented to provide position commands (delayed by one half cycle) for the powered prosthesis. The obvious drawback to such an approach is that the sound-side (or unaffected) leg must be instrumented, which requires the user to don and doff additional equipment and associated wiring. The echo control approach also restricts the use of the prosthesis to unilateral amputees and also presents a problem for “odd” numbers of steps, in which an echoed step is undesirable. A more subtle, although perhaps more significant shortcoming of the echo-type approach is that suitable motion tracking requires a high output impedance of the prosthesis, which forces the amputee to react to the limb rather than interact with it. Specifically, in order for the prosthesis to dictate the joint trajectory, it must assume a high output impedance (i.e., must be stiff), thus precluding any dynamic interaction with the user and the environment, which is in turn contrary to the way in which humans interact with their native limbs.

5. Decomposition-Based Control

This work offers an alternative control which employs the non-invasive MSI approach and obviates the need for sound side instrumentation. Figure 3-2 shows the structure of the proposed control system for the powered prosthesis. In the figure, the feedback loop for each joint incorporates the open loop joint dynamics and the decomposed passive impedance behavior, specified by the function $\tau_p = f_p(\theta, \dot{\theta})$. The input to the feedback loop is an active torque component, which is a function of the user input measured by the socket load cell and specified by the function $\tau_a = f_a(F_S)$.

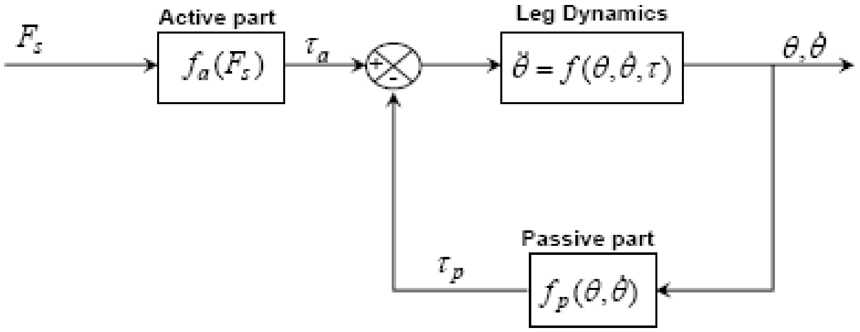

Figure 3-2. Structure of the transfemoral prosthesis control system.

One of the most significant aspects of the proposed controller is the inherent passivity of its structure. Specifically, because the behavior of the leg is decomposed into an active portion that is superimposed upon an underlying passive impedance, and because the active component is a function solely of the user's input, the overall device behavior is guaranteed to be passive. As shown in Figure 3-2, since the function $f_p(\boldsymbol{\theta},\dot{\boldsymbol{\theta}})$ represents a passive mapping from $\boldsymbol{\theta}$ and $\dot{\boldsymbol{\theta}}$ to $\boldsymbol{\tau}_p$ (by definition of the mapping), and since the natural leg dynamics from $\boldsymbol{\tau}$ to $\boldsymbol{\theta}$ and $\dot{\boldsymbol{\theta}}$ are also passive, passivity theory guarantees that the closed-loop formed by these two mappings is also passive (Slotine 1991). As such, the closed-loop portion of the device simply reacts to the user's input, much the way a state-of-the-art passive prosthesis does. The only non-passive (i.e., active) portion of the controller is the component of torque directly resulting from the user's input (i.e., from the socket interaction forces), over which the user has instantaneous and direct control The proposed controller therefore creates a highly stable device over which the human has complete and reliable control. Alternatively stated, because of the structure of the proposed controller, the prosthesis simply reacts to what the user does to it, and as such will form a natural extension of the user.

In the remaining part of the paper, the active passive decomposition method will be explained and the joint torque reference generation procedure is presented. Finally, simulation results based on measured biomechanical data validate the effectiveness of the proposed approach.

6. Active Passive Torque Decomposition

Passive joint torque, τ_p , is defined as the part of the joint torque, τ , which can be represented using spring and dashpot constitutional relationships (passive impedance behavior). The system can only store or dissipate energy due to this component. The active part can be interpreted as the part which supplies energy to the system and the active joint torque is defined as $\tau_a = \tau - \tau_p$. This active part will be represented as an algebraic function of the user input via the MSI (i.e socket interface forces and torques).

Gait can be considered a mainly periodic phenomena with the periods corresponding to the strides. Hence, the decomposition of a stride will give the required active and passive torque mappings for a specific gait mode. In general, the joint behavior exhibits varying active and passive behavior in each stride. Therefore, segmenting of the stride in several parts is necessary. In this case, decomposition of the torque over the entire stride period requires the decomposition of the different segments and piecewise reconstruction of the entire segment period. In order to maintain passive behavior, however, the segments cannot be divided arbitrarily, but rather can only be segmented when the stored energy in the passive elastic element is zero. This requires that the phase space can only be segmented when the joint angle begins and ends at the same value. Figure 3-3 shows the phase portrait of normal speed walking and the four different stride segments, S_1, S_2, S_3 and S_4. Thus, the entire decomposition process consists of first appropriate segmentation of the joint behavior, followed by the decomposition of each segment into its fundamental passive and active components.

The decomposition of each segment shown in Figure 3-3 is converted to an optimization problem. In each segment of the stride, *2n* data points are selected by sampling the angular position in equal intervals between its minimum and maximum and selecting the corresponding positive and negative angular velocities. In this work, the number of angular position samples for each segment, *n* is set to be 100. The constrained least squares optimization problem given in (1) is constructed and solved.

$$\min_{x} \frac{1}{2}\left\|Cx-d\right\|_2^2 \quad s.t. \quad 0 \le x \tag{1}$$

where C, x and d are defined in (2) and (3) respectively. The indexing of the joint angular position, angular velocity and moment samples are explained via the sketch in Figure 3-4.

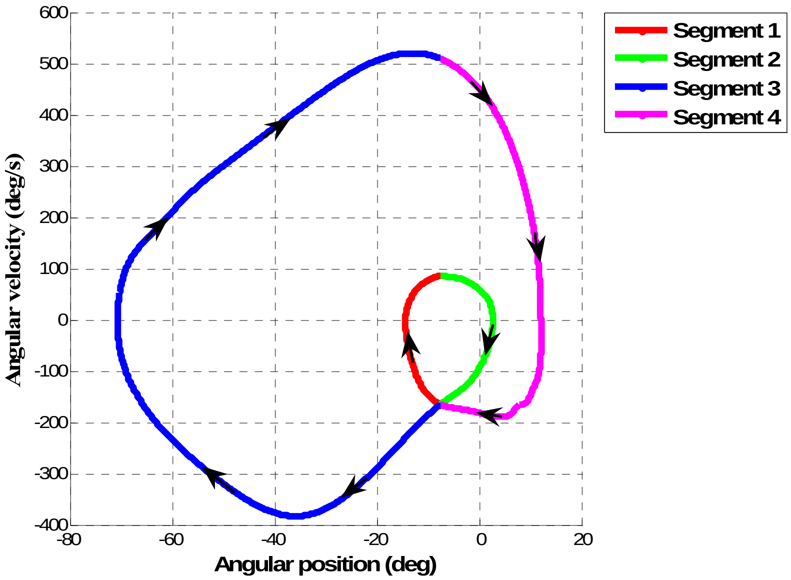

Figure 3-3. Normal speed walking phase portrait of the knee joint and four stride segments.

$$C_{4nx3n} = \begin{bmatrix} C_1 & C_2 & C_3 \end{bmatrix}^T$$

$$C_1 = \begin{bmatrix} diag\left(\begin{bmatrix} \theta_1 \\ \theta_2 \\ \vdots \\ \theta_n \end{bmatrix}_{nx1} - \alpha\right) & \\ & diag\left(\begin{bmatrix} \dot{\theta}_1 \\ \dot{\theta}_2 \\ \vdots \\ \vdots \\ \vdots \\ \dot{\theta}_n \end{bmatrix}_{2nx1}\right) \\ diag\left(\begin{bmatrix} \theta_n \\ \theta_{n-1} \\ \vdots \\ \theta_1 \end{bmatrix}_{nx1} - \alpha\right) & \end{bmatrix}_{2nx3n}$$

$$C_2 = \begin{bmatrix} C_{21} & C_{23} \\ C_{22} & \end{bmatrix}_{2n-1x3n}$$

$$C_{21} = \begin{bmatrix} \theta_1 & -\theta_2 & 0 & \cdots & 0 \\ 0 & \ddots & \ddots & \ddots & \vdots \\ \vdots & \ddots & \theta_{n-1} & \theta_n & 0 \\ 0 & \cdots & 0 & 0 & 0 \end{bmatrix}_{nxn} \qquad (2)$$

$$C_{22} = \begin{bmatrix} \theta_n & -\theta_{n-1} & 0 & \cdots & 0 \\ 0 & \ddots & \ddots & \ddots & \vdots \\ \vdots & \ddots & \theta_3 & -\theta_2 & 0 \\ 0 & \cdots & 0 & \theta_2 & -\theta_1 \end{bmatrix}_{n-1xn}$$

$$C_{23} = \begin{bmatrix} \dot{\theta}_1 & -\dot{\theta}_2 & 0 & \cdots & 0 \\ 0 & \ddots & \ddots & \ddots & \vdots \\ \vdots & \ddots & \dot{\theta}_{2n-2} & -\dot{\theta}_{2n-1} & 0 \\ 0 & \cdots & 0 & \dot{\theta}_{2n-1} & -\dot{\theta}_{2n} \end{bmatrix}_{2n-1x2n}$$

$$C_3 = \begin{bmatrix} \beta & \beta & \cdots & \cdots & \cdots & \beta & \beta \end{bmatrix}_{1x3n}$$

$$x_{3nx1} = \begin{bmatrix} k_1 \\ k_2 \\ \vdots \\ k_{n-1} \\ k_n \\ b_1 \\ b_2 \\ \vdots \\ b_{2n-1} \\ b_{2n} \end{bmatrix}$$

$$d_{4nx1} = \begin{bmatrix} \tau_1 \\ \tau_2 \\ \vdots \\ \tau_{2n-1} \\ \tau_{2n} \\ \tau_1 - \tau_2 \\ \tau_2 - \tau_3 \\ \vdots \\ \tau_{2n-1} - \tau_{2n} \\ 0 \end{bmatrix} \qquad (3)$$

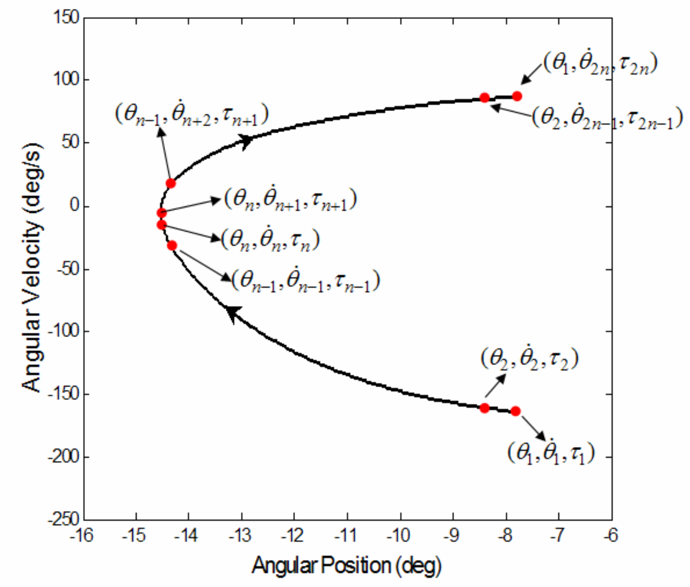

Figure 3-4. Selection and indexing of data samples from Segment 1.

The matrix C consists of three sub-matrices, C_1, C_2 and C_3. C_1 is the main part responsible for the fitting of the spring and dashpot constants, *k* and *b*. C_2 bounds the rate of change of the passive joint torque and ensures smoothness in the resulting passive joint torque, and C_3 is basically a row of penalty constants, β, which penalizes large values of the spring and dashpot constants and thus limits the magnitudes of both. In this work, β is set to 0.1.

The origin of each virtual spring is also added to the optimization problem formulation as a parameter in order to obtain a tighter passive torque fit. Therefore, the optimization problem given by (2) will be solved iteratively for a range of values of spring origin constant, α. The solution with the least error norm is selected as the optimal solution.

The result of the above stated constrained optimization problem for segment 1 is shown in Figure 3-5. As can be seen from the figure, the decomposed passive part is very similar to the joint torque, and thus it can be stated that the behavior of the joint is mainly passive. The result of the decomposition for the segment S_i is stored in R_i of the form given in (4).

$$R_i = \begin{bmatrix} \theta & \dot{\theta} & \tau_{pas} & F_{S1} & F_{S2} & \tau_{act} \end{bmatrix}_{2nx6} \tag{4}$$

$$\tau_{pas} = C_1 x \tag{5}$$

7. Joint Torque Reference Generation

The procedure presented in the previous section decomposes the joint torques into active and passive parts. The joint torque references for the control of the prosthesis are generated by combining this active and passive torques. There are two major challenges to be solved. Firstly, the correct motion segment must be selected. Secondly, after the motion segment is selected at each sampling instant a new joint torque reference should be generated using the discrete mappings for the active and passive torque parts.

A switching system modeling approach incorporating both discrete and continuous states is used for the reconstruction of the torque reference signal. The state chart shown in Figure 3-6 will govern the discrete dynamics of the controller. Since the sequence of the segments is ordered (i.e., the direction of the motion for a specific gait mode does not change), each segment can transition only to the next one, where the transition guard function can be written as a inequality in terms of θ and $\dot{\theta}$. The transitions between segments take no time and the dynamics of the controller are governed by the $\{f_{p_i}(\theta,\dot{\theta})\,;\,f_{a_i}(F_S)\}$ pair at each sampling instant. The joint reference torque is

$$\tau_{ref} = \tau_a + \tau_p = f_{p_i}(\theta,\dot{\theta}) + f_{a_i}(F_S) \tag{6}$$

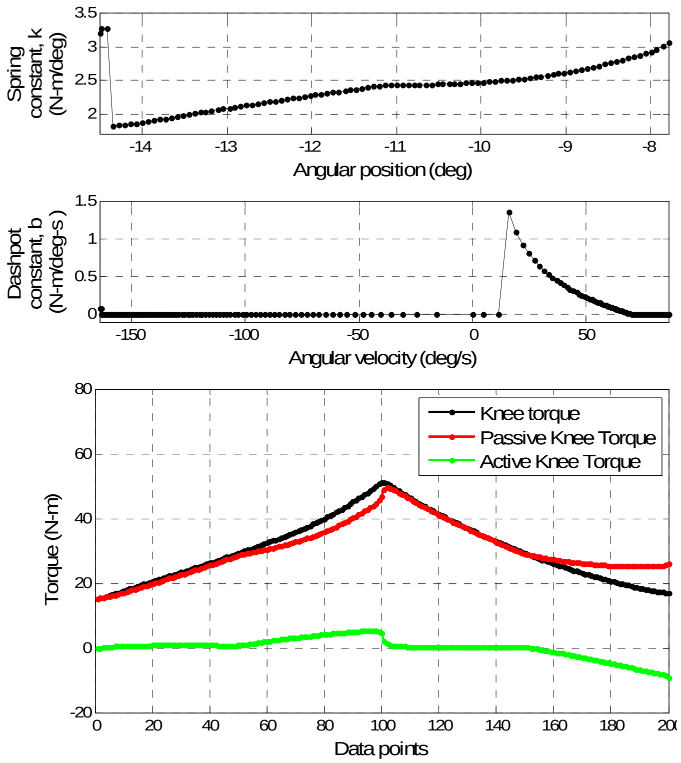

Figure 3-5. The output of the decomposition for Segment 1 showing the spring and dashpot constants and the active and passive knee torques (Spring origin, α .is 23 degrees.).

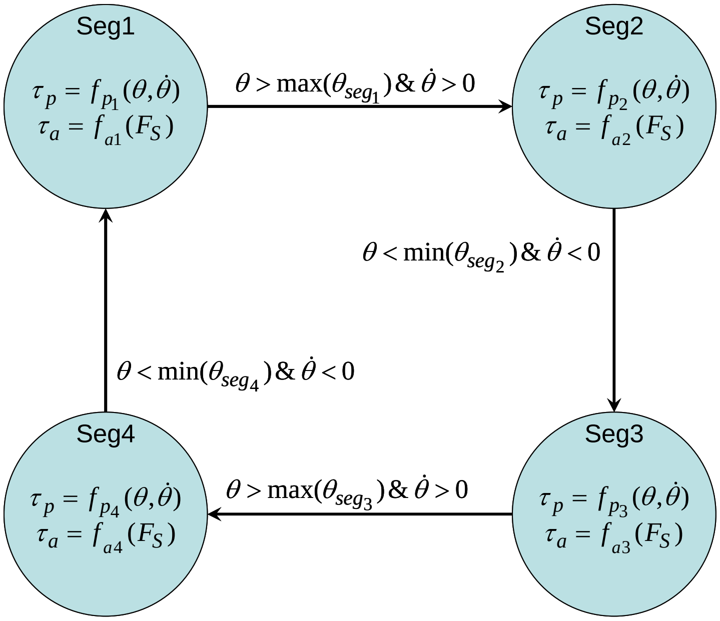
Seg1
$\tau_p = f_{p_1}(\theta,\dot{\theta})$
$\tau_a = f_{a1}(F_S)$
Seg2
$\tau_p = f_{p_2}(\theta,\dot{\theta})$
$\tau_a = f_{a2}(F_S)$
Seg3
$\tau_p = f_{p_3}(\theta,\dot{\theta})$
$\tau_a = f_{a3}(F_S)$
Seg4
$\tau_p = f_{p_4}(\theta,\dot{\theta})$
$\tau_a = f_{a4}(F_S)$
$\theta > \max(\theta_{seg_1})\,\&\,\dot{\theta} > 0$
$\theta < \min(\theta_{seg_2})\,\&\,\dot{\theta} < 0$
$\theta > \max(\theta_{seg_3})\,\&\,\dot{\theta} > 0$
$\theta < \min(\theta_{seg_4})\,\&\,\dot{\theta} < 0$

Figure 3-6. Structure of the switched control system.

The decomposition algorithm presented in this work gives the result matrix, R, for each segment. The discrete data in R is used to construct the joint torque reference for the continuous measurements of another trial in the same gait mode. At each sampling instant of the algorithm, the measurement vector $m=[\theta_m, \dot{\theta}_m, F_{S1\_m}, F_{S2\_m}]^T$ will be acquired. For the reconstruction of the passive knee torque part, the Euclidian error norm between the $[\theta_m \quad \dot{\theta}_m]^T$ and the angular position and velocities of all the samples in that segment $[\theta_i \quad \dot{\theta}_i]^T$ is calculated as shown in (7) and stored in the vector e.

$$e_i = \sqrt{(\theta_m - \theta_i)^2 + (\dot{\theta}_m - \dot{\theta}_i)^2} \tag{7}$$

Then two elements of this vector with the least error norm are found and the passive knee torque reference is found as a weighted linear combination of the passive knee torques corresponding to these points. The reconstruction of the active knee torque part is similar where only $\{\theta, \dot{\theta}, \tau_{pas}\}$ is changed with $\{F_{S1}, F_{S2}, \tau_{act}\}$.

8. Implementation and Experimental Validation

In order to generate appropriate kinematic and kinetic data for the design of the controller and for testing of the approach, gait experiments were conducted in the Biomechanics and Sports Medicine Laboratory of the University of Tennessee at Knoxville. The experimental setup consisted of a 7-camera 240 Hz VICON MX system and 2 AMTI multiaxis force platforms. As is standard in such a setup, hip, knee and ankle angles were measured via the cameras, the ground reaction force was measured using the multiaxis force plates, and the joint torques and forces were computed in post-processing via inverse dynamics, based on inertial parameters estimated with lookup tables. The sampling rate for the cameras and the force plates were 100 Hz and 1000 Hz, respectively. Data collection consisted of four trials each slow walking (WS), normal walking (WN) and fast walking (WF). For the slow, normal, and fast walking, the subject was asked to walk at those respective rates, while an optical interrupt timing system measured the walking speed between the subject's entrance and exit of the camera viewing volume. The minimum, maximum and average speeds for each class of walking speeds are shown in Table 3-1. The experimental setup and the human subject are shown during a measurement trial in Figure 3-7. Figure 3-8 shows the angular position, angular velocity and torque of the knee joint for a walking experiment with normal speed.

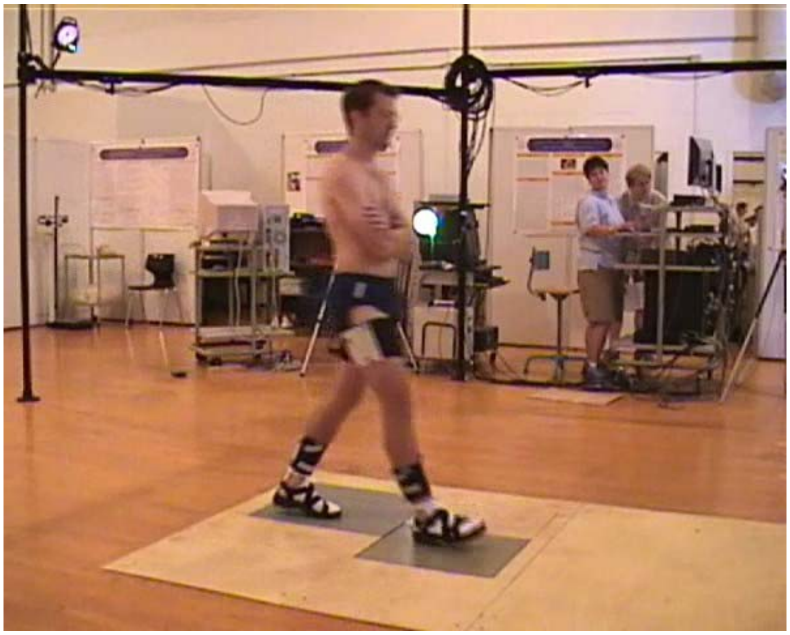

Figure 3-7. Data collection for the demonstration of the proposed approach.

TABLE 3-1

WALKING EXPERIMENT PARAMETERS

Walking Mode	Minimum Speed (m/s)	Average Speed (m/s)	Maximum Speed (m/s)
Slow	1.01	1.04	1.07
Normal	1.19	1.22	1.26
Fast	1.45	1.51	1.56

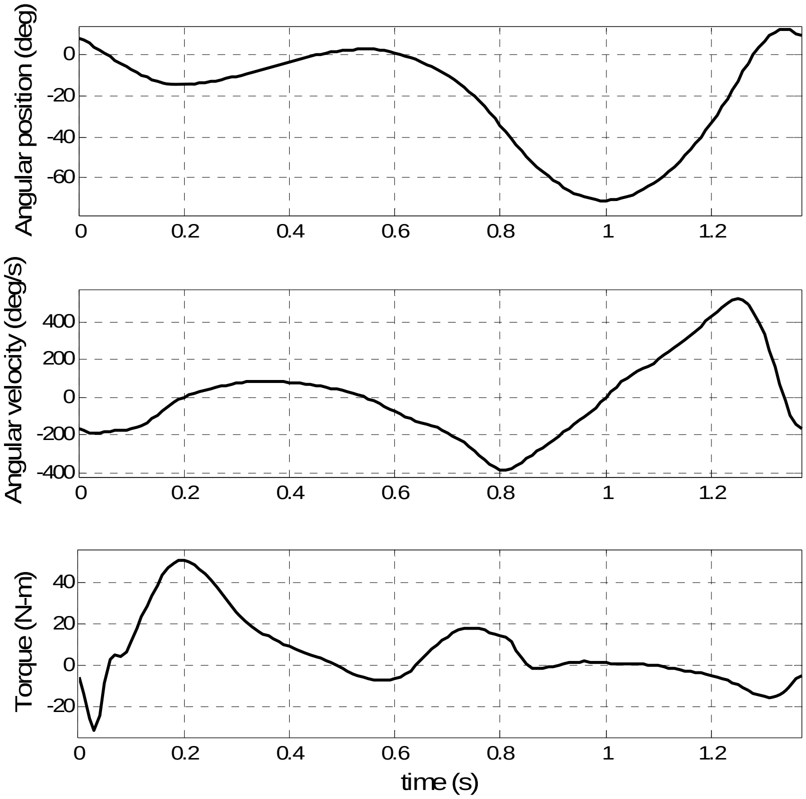

Figure 3-8. The angular position, angular velocity and torque of the knee joint for a walking experiment with normal speed.

9. Results and Discussion

The code for the decomposition algorithm and reconstruction is implemented in Matlab. One stride of the normal walking experiment data is decomposed and the result matrix R is acquired. Then using R, the knee joint torque reference for another trial of the gait data is represented by the structure shown in Figure 3-2. Instead of the socket interface forces, the ground reaction force and the hip moment are used.

The original knee torque and the reconstructed knee torque reference are shown in Figure 3-9(a). As can be observed from the figure, the reconstructed knee torque trajectory is a good approximation of the original knee torque. Figure 3-9(b) shows the angular velocity versus the knee torque. The loops in the original knee torque versus angular position plot are also present in the reconstructed knee torque reference versus angular position plot. This shows that the active passive decomposition preserves the energetic behavior of the system.

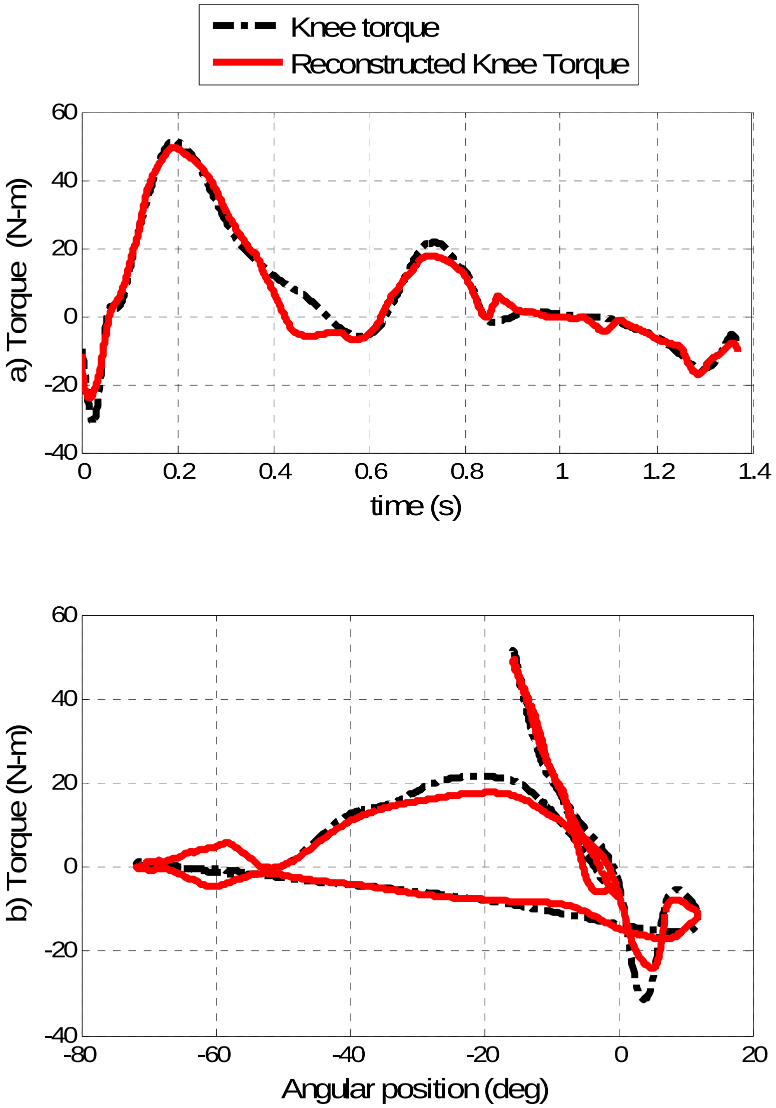

Figure 3-9. Original knee torque and the reconstructed knee torque reference versus time (a) and the angular position (b).

10. Conclusion

This paper proposes a method for the control of a powered transfemoral prosthesis. The approach is based on the decomposition of knee torque into 1) a fundamentally passive component, which is an algebraic function of joint angle and angular velocity, and 2) an active component, which is an algebraic function of the measured forces between the user socket and the prosthesis. The paper presents a method for decomposing measured data into these passive and active algebraic functions, and describes a method for generating real-time torque trajectories based on these functions and the measured joint angles and angular velocities and interaction forces. The effectiveness of the approach is demonstrated on measured biomechanical data. Future work will utilize the proposed approach for the real-time control of the powered transfemoral prosthesis.

11. References

Aeyels, B., Van Petegem, W., Sloten, V., Van der Perre, G. and Peeraer, L., EMG-based finite state approach for a microcomputer-controlled above-knee prosthesis, Annual International Conference of the IEEE Engineering in Medicine and Biology, Proceedings of IEEE Engineering in Medicine and Biology, 1995.

DeVita, P., Torry M., Glover, K.L., and Speroni, D.L. A Functional Knee Brace Alters Joint Torque and Power Patterns during Walking and Running, Journal of Biomechanics, vol. 29, no. 5, pp. 583-588, 1996.

Donath, M., Proportional EMG Control for Above-Knee Prosthesis', Department of Mechanical Engineering Masters Thesis, MIT, 1974.

Fite, K.B., Mitchell, J., Barth, E.J., and Goldfarb, M. A Unified Force Controller for a Proportional-Injector Direct-Injection Monopropellant-Powered Actuator, ASME Journal of Dynamic Systems, Measurement and Control, vol. 128, no. 1, pp. 159-164, 2006.

Fite, K.B., and Goldfarb, M. Design and Energetic Characterization of a Proportional-Injector Monopropellant-Powered Actuator, IEEE/ASME Transactions on Mechatronics, vol. 11, no. 2, pp. 196-204, 2006.

Flowers, W.C., A Man-Interactive Simulator System for Above-Knee Prosthetics Studies, Department of Mechanical Engineering PhD Thesis, MIT, 1973.

Flowers, W.C., and Mann, R.W. Electrohydraulic knee-torque controller for a prosthesis simulator. ASME Journal of Biomechanical Engineering, vol. 99, no. 4, pp. 3-8, 1977.

Goldfarb, M., Barth, E.J., Gogola, M.A., and Wehrmeyer, J.A.. Design and Energetic Characterization of a Liquid-Propellant-Powered Actuator for Self-Powered Robots, IEEE/ASME Transactions on Mechatronics, vol. 8, no. 2, pp. 254-262, 2003.

Grimes, D. L. An Active Multi-Mode Above Knee Prosthesis Controller. Department of Mechanical Engineering PhD Thesis, MIT, 1979.

Grimes, D. L., Flowers, W. C., and Donath, M. Feasibility of an active control scheme for above knee prostheses. ASME Journal of Biomechanical Engineering, vol. 99, no. 4, pp. 215-221, 1977.

Jacobs, R., Bobbert, M.F., van Ingen Schenau, G.J. Mechanical output from individual muscles during explosive leg extensions: the role of biarticular muscles. Journal of Biomechanics, vol. 29, no. 4, pp. 513-523, 1996.

Myers, D. and Moskowitz, G., Myoelectric pattern recognition for use in the volitional control of above-knee prosthesis, IEEE Trans. Syst. Man Cybern., Vol. SMC-11 No. 4, pp. 296-302, 1981.

Myers, D. and Moskowitz, G., Active EMG-controlled A/K prosthesis. Control aspects of prosthetics and orthotics, Proceedings of the IFAC Symposium, Columbus, OH, 1983.

Nadeau, S., McFadyen, B.J., and Malouin, F. Frontal and sagittal plane analyses of the stair climbing task in healthy adults aged over 40 years: What are the challenges compared to level walking? Clinical Biomechanics, vol. 18, no. 10, pp. 950-959, 2003.

Nagano, A., Ishige, Y., and Fukashiro, S. Comparison of new approaches to estimate mechanical output of individual joints in vertical jumps. Journal of Biomechanics, vol. 31, no. 10, pp. 951-955, 1998.

Prilutsky, B.I., Petrova, L.N., and Raitsin, L.M. Comparison of mechanical energy expenditure of joint moments and muscle forces during human locomotion. Journal of Biomechanics, vol. 29, no. 4, pp. 405-415, 1996.

Popovic, D. and Schwirtlich, L. Belgrade active A/K prosthesis, in de Vries, J. (Ed.), Electrophysiological Kinesiology, Intern. Congress Ser. No. 804, Excerpta Medica, Amsterdam, The Netherlands, pp. 337–343, 1988.

Riener, R., Rabuffetti, M., and Frigo, C. Joint powers in stair climbing at different slopes. Proceedings of the IEEE International Conference on Engineering in Medicine and Biology, vol. 1, p. 530, 1999.

Shields, B.L., Fite, K., and Goldfarb, M. Design, Control, and Energetic Characterization of a Solenoid Injected Monopropellant Powered Actuator, IEEE/ASME Transactions on Mechatronics, vol. 11, no. 4, pp. 477-487, 2006.

Stein, J.L. Design Issues in the Stance Phase Control of Above-Knee Prostheses. Department of Mechanical Engineering PhD Thesis, MIT, 1983

Stein, J.L., and Flowers, W.C. Stance phase control of above-knee prostheses: knee control versus SACH foot design.   Journal of Biomechanics, vol. 20, no. 1, pp. 19-28, 1987.

Slotine, J.J.E., and Li, W., Applied Nonlinear Control, Prentice-Hall, 1991.

Sup, F., and Goldfarb, M. Design of a Pneumatically Actuated Transfemoral Prosthesis. Proceedings of ASME International Mechanical Engineering Conference and Exposition, IMECE2006-15707, 2006.

Triolo, R. and Moskowitz, G., Autoregressive EMG analysis and prosthetic control, Proceedings of the 35th Annual Conference on Engineering in Medicine and Biology, Philadelphia, PA, 1982.

Winter, D.A. The biomechanics and motor control of human gait: normal, elderly and pathological, University of Waterloo Press, 2nd ed, 1991.

Winter, D. A. and Sienko, S. E. Biomechanics of below-knee amputee gait. J. Biomechanics. 21, 361–367, 1988.

CHAPTER IV

THREE AXIS SOCKET LOAD CELL CALIBRATION

The proposed control algorithm for the powered prosthesis determines the user intent based on the characteristic shape of the force and moment vector of interaction between the user and prosthesis. Moreover, the active passive decomposition based control for generating the joint torques uses the force and moment vector in order to map the active part of the joint torques. Therefore, the precise measurement of the force and moment vector is a very critical task for the control performance of the whole powered prosthesis. This force and moment vector is measured by a three axis socket load cell, which is stationed just above the knee. It measures the sagittal plane moment, M_S , frontal plane moment, M_F , and the vertical axial load, F , above the knee. Due to the interaction of different forces and moments, calibration is necessary in order to make precise measurements. For the calibration of the socket load cell, an experimental setup consisting of two orthogonal bars is constructed. The socket load cell is at the intersection of the two bars. One of the bars is connected to two pneumatic pistons which can exert different forces and moments on a plane to the load cell. The other bar can exert different moments and forces to the load cell by changing the weights on the bar (See Figure 4-1).

576 measurements ranging from -400N to 1100N for the axial load, -50Nm to 50Nm for the frontal plane moment and -120Nm to 120Nm for the sagittal plane moment is done. The analog outputs for the three measurement channels are recorded using Matlab/Simulink and data acqusition board. First order linear least square fits were fit to the raw data using the standard definition for least squares:

$$\theta = \left(\Phi^T \cdot \Phi\right)^{-1} \cdot Y \tag{1}$$

where,

$$\Phi = \begin{pmatrix} F^0 \\ M_F \\ F \\ M_S \end{pmatrix} \tag{2}$$

and

$$Y = \begin{pmatrix} F & M_F & M_S \end{pmatrix} \tag{3}$$

Using the calibration data in the linear least squares equation the following matrix results:

$$\theta = \begin{pmatrix} 163.4 & -5.1 & 30.6 \\ -16.1 & -23.4 & -0.9 \\ -83.6 & -0.5 & -0.2 \\ -3.7 & -0.4 & 21.1 \end{pmatrix} \tag{4}$$

The results for the axial load, frontal plane moment and sagittal plane moment are shown in Figure 4-2 to Figure 4-4, respectively. It is seen that the square root of the mean squared error is 81.6 N for the axial load measurement, 3.9 Nm for the sagittal plane moment measurement and 1.9 Nm for the frontal plane moment measurement. It is also observed that higher order fits to the raw data does not increase the fitting accuracy substantially and it is decided to use the first order linear fitting.

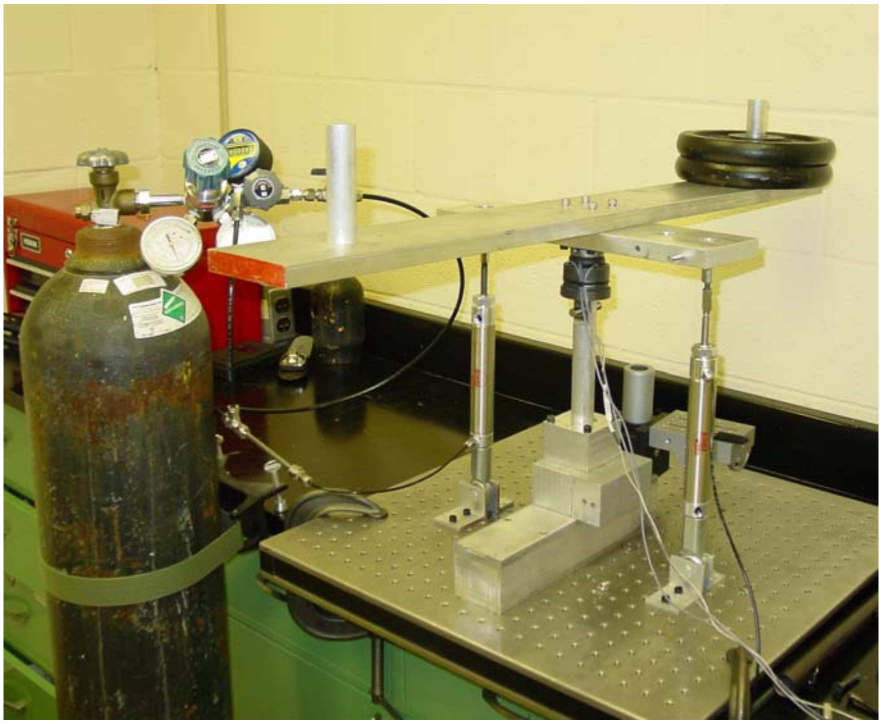

Figure 4-1. Three axis socket load cell calibration setup

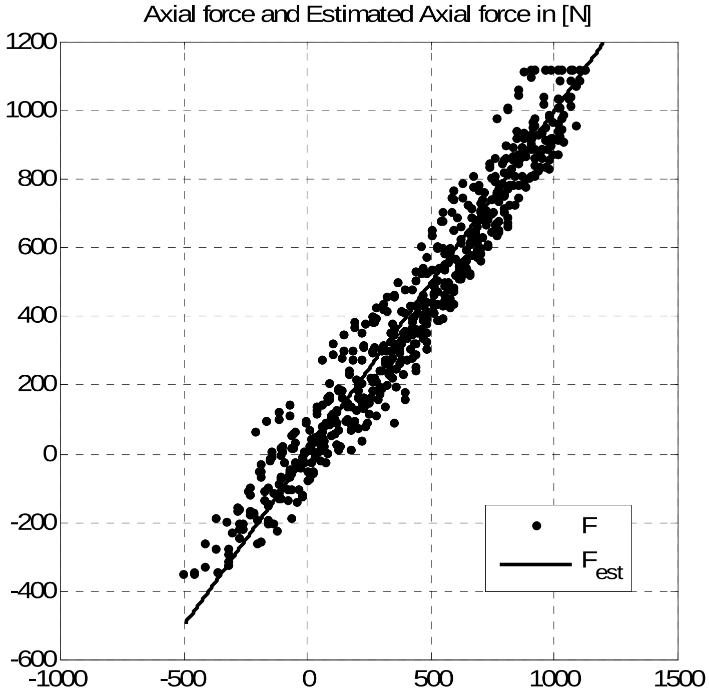

Figure 4-2. Axial force versus Estimated Axial Force

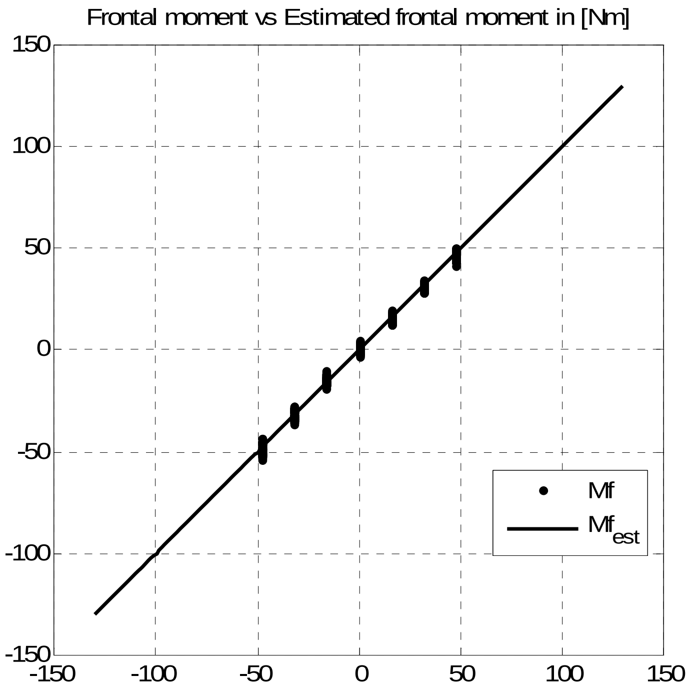

Figure 4-3. Frontal moment versus Estimate frontal moment.

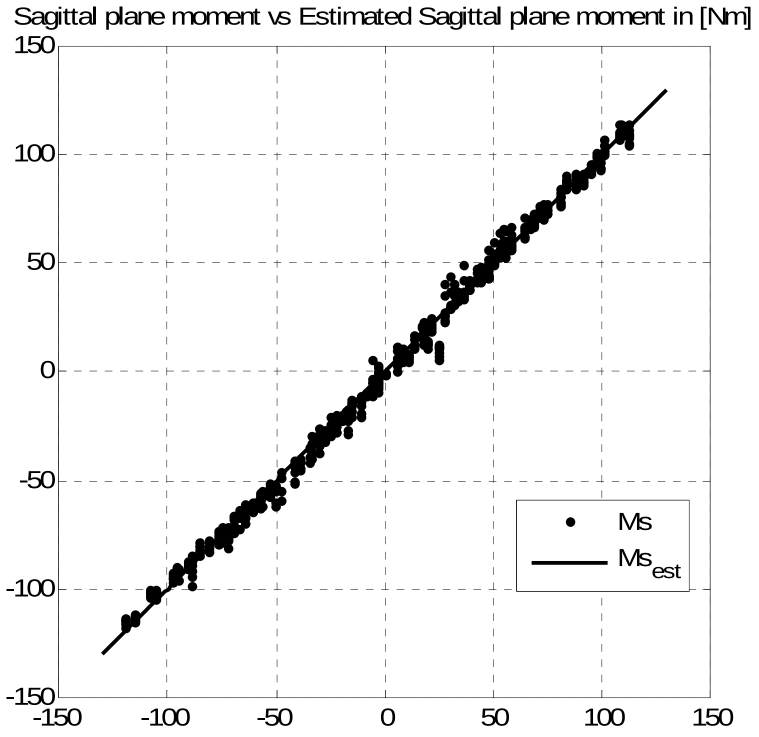

Figure 4-4. Sagittal plane moment versus estimated sagital plane moment.

APPENDIX A

MATLAB CODES

1. K-Nearest Neighbor Algorithm Main Script

```
%% Robotic Leg Intent Recognizer Design
% Author: Atakan Varol

% Clean the environment
clc, clear, close all, warning off

%% Generate the walking data struct for datasets from expriment measurements
sm_const = 3;
[mg, n] = create_experiment(sm_const);

%% K-Nearest Neighbor Intent Recognition Code

% Trial dataset name array
trial_set_list = ['wsl_tr1'; 'wsl_tr2'; 'wsl_tr3'; 'wsl_tr4'; ... % 1  2  3  4
    'wno_tr1'; 'wno_tr2'; 'wno_tr3'; 'wno_tr4'; ...               % 5  6  7  8
    'wfa_tr1'; 'wfa_tr2'; 'wfa_tr3'; 'wfa_tr4'; ...              % 9  10 11 12
    'w2s_tr1'; 'w2s_tr2'; 's2w_tr1'; 's2w_tr2'; 'sta_tr1'];    % 13 14 15 16 17

% Museum Walking Scenario
trial_sets = [17 15 1 2 5 6 9 10 11 12 7 8 3 4 5 6 1 2 13 17];

% Create the trial set
trial_data_lc1 = [];
trial_data_lc2 = [];
trial_data_ankpos = [];
trial_data_knepos = [];
mode_real = [];

for ind = 1: length(trial_sets)
    trial_data_lc1 = [ trial_data_lc1; eval(['mg.',
trial_set_list(trial_sets(ind),:), '.lc1'])];
    trial_data_lc2 = [ trial_data_lc2; eval(['mg.',
trial_set_list(trial_sets(ind),:), '.lc2'])];
    trial_data_knepos = [ trial_data_knepos; eval(['mg.',
trial_set_list(trial_sets(ind),:), '.knepos'])];
```

```
    trial_data_ankpos = [ trial_data_ankpos; eval(['mg.',
trial_set_list(trial_sets(ind),:), '.ankpos'])];

    % Create the real mode vector
    if trial_sets(ind) <= 4
        mode_real = [mode_real; 2*ones(length(eval(['mg.',
trial_set_list(trial_sets(ind),:), '.lc1'])),1)];
    elseif trial_sets(ind) <= 8
        mode_real = [mode_real; 3*ones(length(eval(['mg.',
trial_set_list(trial_sets(ind),:), '.lc1'])),1)];
    elseif trial_sets(ind) <= 12
        mode_real = [mode_real; 4*ones(length(eval(['mg.',
trial_set_list(trial_sets(ind),:), '.lc1'])),1)];
    elseif trial_sets(ind) <= 14
        mode_real = [mode_real; linspace(2,1,length(eval(['mg.',
trial_set_list(trial_sets(ind),:), '.lc1'])))'];
    elseif trial_sets(ind) <= 16
        mode_real = [mode_real; linspace(1,2,length(eval(['mg.',
trial_set_list(trial_sets(ind),:), '.lc1'])))'];
    elseif trial_sets(ind) <= 17
        mode_real = [mode_real; 1*ones(length(eval(['mg.',
trial_set_list(trial_sets(ind),:), '.lc1'])),1)];
    end
end
% Normalize the trial data
trial_data_lc1_norm = smooth(trial_data_lc1/ n.lc1,2);
trial_data_lc2_norm = smooth(trial_data_lc2/ n.lc2,2);
trial_data_knepos_norm = smooth(trial_data_knepos/ n.knepos,2);
trial_data_ankpos_norm = smooth(trial_data_ankpos/ n.ankpos,5);

% Particle filter parameter initialization
p = 16;                  % # of points in one frame for time based majority voting
k = 7;                   % # of nearest neighbours
alpha  = 3;              % threshold level adjustment constant
cost_norm = 1;           % 1 --> abs norm;  2 --> euclidian norm
sim_time = length(trial_data_lc1);   % Total simulation time steps
t = 1;                               % Initial time
disp_int = 100;                      % interval between data displays

mode_frame = zeros(p,1);
```

```
%Prepare the data matrix
mg.dataset_list = ['ws1'; 'ws2';'ws3';  'wn1'; 'wn2';'wn4'; 'wf1'; 'wf2'; 'wf3';
'st1'];
dataset_len = [];
dataset_lc1_arr = []; dataset_lc2_arr = [];
dataset_knepos_arr = []; dataset_ankpos_arr = [];
for t =  1 : length(mg.dataset_list)
    dataset_len = [dataset_len, eval(['mg.' , mg.dataset_list(t,:),'.len'])];
    dataset_lc1_arr = [dataset_lc1_arr; eval(['mg.' ,
mg.dataset_list(t,:),'.lc1_norm'])];
    dataset_lc2_arr = [dataset_lc2_arr; eval(['mg.' ,
mg.dataset_list(t,:),'.lc2_norm'])];
    dataset_knepos_arr = [dataset_knepos_arr; eval(['mg.' ,
mg.dataset_list(t,:),'.knepos_norm'])];
    dataset_ankpos_arr = [dataset_ankpos_arr; eval(['mg.' ,
mg.dataset_list(t,:),'.ankpos_norm'])];
end

% KNN Algorithm main loop
for t = 1:sim_time

    % Cost calculation
    if cost_norm == 1   % abs norm
        cost =  abs(trial_data_lc1_norm(t) - dataset_lc1_arr) + ...
            abs(trial_data_lc2_norm(t) - dataset_lc2_arr) + ...
            abs(trial_data_knepos_norm(t) - dataset_knepos_arr) + ...
            abs(trial_data_ankpos_norm(t) - dataset_ankpos_arr);
    elseif cost_norm == 2 % euclidian norm
        cost = sqrt(  (trial_data_lc1_norm(t) -dataset_lc1_arr).^2 + ...
            (trial_data_lc2_norm(t) - dataset_lc2_arr).^2 + ...
            (trial_data_knepos_norm(t) - dataset_knepos_arr).^2 + ...
            (trial_data_ankpos_norm(t) -  dataset_ankpos_arr).^2);
    end

    % Mode estimation for the iteration
    [cost_val, cost_ind] = sort(cost);
    mode = zeros(4,1); % 1 --> standing ; 2 --> slow; 3 --> medium; 4 --> fast
    for ind = 1:k
        if cost_ind(ind) <= sum(dataset_len(1:3))
            mode(2) = mode(2) + 1;
        elseif cost_ind(ind) <= sum(dataset_len(1:6))
```

```
            mode(3) = mode(3) + 1;
        elseif cost_ind(ind) <= sum(dataset_len(1:9))
            mode(4) = mode(4)+ 1;
        elseif cost_ind(ind) <= sum(dataset_len(1:10))
            mode(1) = mode(1) + 1;
        end
    end
    [dum mode_est_plain(t)] = max(mode);

    % Hysteresis
    if ( t > 1)
        mode(mode_est_iter(t-1)) = (alpha*mode( mode_est_iter(t-1)));
    end
    [dum mode_est_iter(t)] = max(mode);    % Select the mode with the most
neighbour count

    % Majority vote
    mode_frame(2:p) = mode_frame(1:p-1);
    mode_frame(1) = mode_est_iter(t);
    mode_est_gen(t) = mode_est_iter(t);
    mode = zeros(4,1); % 1 --> standing ; 2 --> slow; 3 --> medium; 4 --> fast
    if ( t >= p)
        for ind = 1:p
            if  mode_frame(ind) == 1
                mode(1) = mode(1) + 1;
            elseif  mode_frame(ind) == 2
                mode(2) = mode(2) + 1;
            elseif mode_frame(ind) == 3
                mode(3) = mode(3) + 1;
            elseif mode_frame(ind) == 4
                mode(4) = mode(4) + 1;
            end
        end
        [dum1 dum2] = max(mode);    % Select the dominant mode in the frame
        mode_est_gen(t) = dum2(1);
    end

    % Display
    if (mod(t,disp_int)==0)
        disp(sprintf('Iteration: %d, Time: %0.5g, Mode: %d',t, t/100,
mode_est_iter(t)))
```

```
    end
end

% Visualization
figure(1);
subplot 311, plot((1:sim_time)/100, mode_real, 'k-',(1:sim_time)/100,
mode_est_plain,'ko')
title('a) Plain K-NN')
ylabel('Gait mode')
axis([0 30.42 0.8 4.2])
subplot 312, plot((1:sim_time)/100, mode_real, 'k-',(1:sim_time)/100,
mode_est_iter,'ko')
title('b) K-NN with biasing constant')
ylabel('Gait mode')
axis([0 30.42 0.8 4.2])
subplot 313, plot((1:sim_time)/100, mode_real, 'k-',(1:sim_time)/100,
mode_est_gen,'ko')
title('c) K-NN with biasing constant and the time based majority voting')
ylabel('Gait mode')
xlabel('time in s')
axis([0 30.42 0.8 4.2])
legend('real mode', 'predicted mode')
```

2. Active-Passive Decomposition Procedure Main Script

```
%% Robotic Leg Control Design
Author: Atakan Varol

% Clean the environment
clc, clear, close all, warning off

%% Generate the walking data struct for datasets from expriment measurements
sm_const = 3;
[mg, n] = create_experiment(sm_const);


%% Active-passive decomposition method 1

len_data_smooth = 100;  % moving average smoothing filter frame size for knepos,
knevel and knemom
epsi = 1e-3;            % very small number
out_const = 10;         % outlier const

% Get the knepos, knevel and knemom -  interpolate them to 10000 points
knepos_int = smooth(interp([mg.wn2.knepos(end-10+1:end) ; mg.wn2.knepos;
mg.wn2.knepos(1:10)] ,100),len_data_smooth);
knevel_int = smooth(interp([mg.wn2.knevel(end-10+1:end) ; mg.wn2.knevel;
mg.wn2.knevel(1:10)] ,100),len_data_smooth);
knemom_int = smooth( interp([mg.wn2.knemom(end-10+1:end) ; mg.wn2.knemom;
mg.wn2.knemom(1:10)] ,100), len_data_smooth);
hipmom_int = smooth( interp([mg.wn2.lc2(end-10+1:end) ; mg.wn2.lc2;
mg.wn2.lc2(1:10)] ,100), 3*len_data_smooth);
gref_int= smooth( interp([mg.wn2.lc1(end-10+1:end) ; mg.wn2.lc1;
mg.wn2.lc1(1:10)] ,100), 3*len_data_smooth);
knevel_int = knevel_int(1001:end-1000);
knepos_int = knepos_int(1001:end-1000);
knemom_int = knemom_int(1001:end-1000);
hipmom_int = hipmom_int(1001:end-1000);
gref_int= gref_int(1001:end-1000);

% Create first linear programming problem (for the first segment)
% Segment 1 with -15 degree angular position offset
```

```
res_norm_hist = [];
for offset_seg1 = -23
    ind_seg1 = 1050:3390;
    knepos_seg1 = knepos_int(ind_seg1);                  % Impose boundary value
    knepos_seg1_offset = knepos_seg1  - offset_seg1;     % For easier
optimization formulation
    knevel_seg1 = knevel_int(ind_seg1);
    knemom_seg1 = knemom_int(ind_seg1);
    max_knepos_seg1 = max(knepos_seg1_offset);
    min_knepos_seg1 = min(knepos_seg1_offset);

    tr_len = 100;
    knepos_seg1_trial = linspace( max_knepos_seg1, min_knepos_seg1, tr_len);
    delta = abs(knepos_seg1_trial(2) -  knepos_seg1_trial(1));

    knemom_lp_seg1 = zeros(2*tr_len+1,1);
    mat_lp_seg1 = zeros(2*tr_len+1,3*tr_len);

    posind_hist = zeros(tr_len,1);
    velind_hist = zeros(2*tr_len,1);
    for t = 1:tr_len
        [ind1_list] = knepos_seg1_offset > knepos_seg1_trial(t) - delta/2  & ...
            knepos_seg1_offset < knepos_seg1_trial(t) + delta/2 & ...
            knevel_seg1 > 0 ;
        ind1 = find(ind1_list == 1, 1, 'first');
        posind_hist(t) = ind1;
        velind_hist(t) = ind1;

        [ind2_list] = knepos_seg1_offset > knepos_seg1_trial(t) - delta/2  & ...
            knepos_seg1_offset < knepos_seg1_trial(t) + delta/2 & ...
            knevel_seg1 < 0;
        ind2 = find(ind2_list == 1, 1, 'last');
        velind_hist(2*tr_len + 1 - t) = ind2;
    end
    posind_hist = posind_hist(end:-1:1);
    velind_hist = velind_hist(end:-1:1);
    knemom_lp_seg1 = [ knemom_seg1(velind_hist); ...
        knemom_seg1(velind_hist(1:end-1)) -  knemom_seg1(velind_hist(2:end)) ;
0];
    mat_lp_seg1 = [ [ diag(knepos_seg1_offset(posind_hist));
diag(knepos_seg1_offset(posind_hist(end:-1:1))) ], ...
```

```
        diag(knevel_seg1(velind_hist))];
    mat_lp_seg1 = [mat_lp_seg1 ; [ mat_lp_seg1(1:end-1,:) -
mat_lp_seg1(2:end,:)]];
    mat_lp_seg1 = [mat_lp_seg1 ; 0.2*ones(1,300)];
    options = optimset('MaxIter', 2e3);
    [kb_list_seg1 res_norm res eflag] = lsqlin(mat_lp_seg1, knemom_lp_seg1, [],
[],[],[],zeros(300,1),100*ones(300,1),[],options) ;
    kb_list_seg1(kb_list_seg1 < epsi) = 0;
    k_seg1 = kb_list_seg1(1:100);
    b_seg1 = kb_list_seg1(101:300);
    knemom_fit_seg1  = mat_lp_seg1(1:end-2*tr_len,:)*kb_list_seg1(1:end);

    res_norm_hist = [res_norm_hist res_norm];
end
[val, ind ] = min(res_norm_hist)
indlist_gen = [];
indlist_gen = [indlist_gen ; (1049 + velind_hist)];
indlist_seg1 = 1049+velind_hist;

figure(1),
subplot 311, plot(knepos_seg1(posind_hist), k_seg1, 'r.-'),
ylabel('Spring constant, k'),
xlabel('Angular position (deg)'), axis tight, grid on
subplot 312, plot(knevel_seg1(velind_hist), b_seg1, 'r.-'),
ylabel('Dashpot constant, k'),
xlabel('Angular position (deg)'), axis tight, grid on
subplot 313, plot(1:length(knemom_lp_seg1)-2*tr_len,
knemom_lp_seg1(1:end-2*tr_len) , 'r.',...
    1:length(knemom_lp_seg1)-2*tr_len, knemom_fit_seg1, 'g.','LineWidth',2),
grid on

% Create the second linear programming problem (for the second segment)
% Segment 2 with -15 degree angular position offset
res_norm_hist = [];
for offset_seg2 = -23
    ind_seg2 = 3391:6830;
    knepos_seg2 = knepos_int(ind_seg2);          % Impose boundary value
knepos_seg2_offset = knepos_seg2  - offset_seg2; % For easier optimization
formulation
    knevel_seg2 = knevel_int(ind_seg2);
    knemom_seg2 = knemom_int(ind_seg2);
    max_knepos_seg2 = max(knepos_seg2_offset);
    min_knepos_seg2 = min(knepos_seg2_offset);

    tr_len = 100;
    knepos_seg2_trial = linspace( min_knepos_seg2, max_knepos_seg2, tr_len);
    delta = abs(knepos_seg2_trial(2) -  knepos_seg2_trial(1));

    knemom_lp_seg2 = zeros(2*tr_len+1,1);
    mat_lp_seg2 = zeros(2*tr_len+1,3*tr_len);

    posind_hist = zeros(tr_len,1);
    velind_hist = zeros(2*tr_len,1);
    for t = 1:tr_len
        [ind1_list] = knepos_seg2_offset > knepos_seg2_trial(t) - delta/2  & ...
            knepos_seg2_offset < knepos_seg2_trial(t) + delta/2 & ...
            knevel_seg2 > 0 ;
        ind1 = find(ind1_list == 1, 1, 'first');
        posind_hist(t) = ind1;
        velind_hist(t) = ind1;

        [ind2_list] = knepos_seg2_offset > knepos_seg2_trial(t) - delta/2  & ...
            knepos_seg2_offset < knepos_seg2_trial(t) + delta/2 & ...
            knevel_seg2 < 0;
        ind2 = find(ind2_list == 1, 1, 'last');
        velind_hist(2*tr_len + 1 - t) = ind2;
    end
    knemom_lp_seg2 = [ knemom_seg2(velind_hist); ...
        knemom_seg2(velind_hist(1:end-1)) -  knemom_seg2(velind_hist(2:end)) ;
0];
    mat_lp_seg2 = [ [ diag(knepos_seg2_offset(posind_hist));
diag(knepos_seg2_offset(posind_hist(end:-1:1))) ], ...
        diag(knevel_seg2(velind_hist))];
    mat_lp_seg2 = [mat_lp_seg2 ; [ mat_lp_seg2(1:end-1,:) -
mat_lp_seg2(2:end,:)]];
    mat_lp_seg2 = [mat_lp_seg2 ; 0.1*ones(1,300)];
    options = optimset('MaxIter', 2e3);
    [kb_list_seg2 res_norm res eflag] = lsqlin(mat_lp_seg2, knemom_lp_seg2, [],
[],[],[],zeros(300,1),100*ones(300,1),[],options) ;
    kb_list_seg2(kb_list_seg2 < epsi) = 0;
    k_seg2 = kb_list_seg2(1:100);
    b_seg2 = kb_list_seg2(101:300);
    knemom_fit_seg2  = mat_lp_seg2(1:end-2*tr_len,:)*kb_list_seg2(1:end);

    res_norm_hist = [res_norm_hist res_norm];
end
[val, ind ] = min(res_norm_hist)
indlist_gen = [indlist_gen ; (3390 + velind_hist)];
indlist_seg2 = 3390+velind_hist;

figure(2),
subplot 311, plot(knepos_seg2(posind_hist), k_seg2, 'r.-'), title('Segment2
spring values'), axis tight, grid on
subplot 312, plot(knevel_seg2(velind_hist), b_seg2, 'r.-'), title('Segment2
dashpot values1'), axis tight, grid on
subplot 313, plot(1:length(knemom_lp_seg2)-2*tr_len,
knemom_lp_seg2(1:end-2*tr_len) , 'r.',...
    1:length(knemom_lp_seg2)-2*tr_len, knemom_fit_seg2, 'g.','LineWidth',2),
grid on

 % Create the third linear programming problem (for the third segment)
% Segment 3 with -15 degree angular position offset

res_norm_hist = [];
% for offset_seg3 = -25:0
for offset_seg3 = -23
    ind_seg3 =  6831:12614;
    knepos_seg3 = knepos_int(ind_seg3);                  % Impose boundary value
- just for computational purposes
    knepos_seg3_offset = knepos_seg3  - offset_seg3;       % For easier
optimization formulation
    knevel_seg3 = knevel_int(ind_seg3);
    knemom_seg3 = knemom_int(ind_seg3);
    max_knepos_seg3 = max(knepos_seg3_offset);
    min_knepos_seg3 = min(knepos_seg3_offset);

    tr_len = 100;
    knepos_seg3_trial = linspace( max_knepos_seg3, min_knepos_seg3, tr_len);
    delta = abs(knepos_seg3_trial(2) -  knepos_seg3_trial(1));

    knemom_lp_seg3 = zeros(2*tr_len+1,1);
    mat_lp_seg3 = zeros(2*tr_len+1,3*tr_len);
    posind_hist = zeros(tr_len,1);
    velind_hist = zeros(2*tr_len,1);
    for t = 1:tr_len
        [ind1_list] = knepos_seg3_offset > knepos_seg3_trial(t) - delta/2  & ...
            knepos_seg3_offset < knepos_seg3_trial(t) + delta/2 & ...
            knevel_seg3 > 0 ;
        ind1 = find(ind1_list == 1, 1, 'first');
        posind_hist(t) = ind1;
        velind_hist(t) = ind1;

        [ind2_list] = knepos_seg3_offset > knepos_seg3_trial(t) - delta/2  & ...
            knepos_seg3_offset < knepos_seg3_trial(t) + delta/2 & ...
            knevel_seg3 < 0;
        ind2 = find(ind2_list == 1, 1, 'last');
        velind_hist(2*tr_len + 1 - t) = ind2;
    end
    posind_hist = posind_hist(end:-1:1);
    velind_hist = velind_hist(end:-1:1);
    knemom_lp_seg3 = [ knemom_seg3(velind_hist); ...
        knemom_seg3(velind_hist(1:end-1)) -  knemom_seg3(velind_hist(2:end)) ;
0];
    mat_lp_seg3 = [ [ diag(knepos_seg3_offset(posind_hist));
diag(knepos_seg3_offset(posind_hist(end:-1:1))) ], ...
        diag(knevel_seg3(velind_hist))];
    mat_lp_seg3 = [mat_lp_seg3 ; [ mat_lp_seg3(1:end-1,:) -
mat_lp_seg3(2:end,:)]];
    mat_lp_seg3 = [mat_lp_seg3 ; 0.2*ones(1,300)];
    options = optimset('MaxIter', 5e3);
    [kb_list_seg3 res_norm res eflag] = lsqlin(mat_lp_seg3, knemom_lp_seg3, [],
[],[],[],zeros(300,1),100*ones(300,1),[],options) ;
    kb_list_seg3(kb_list_seg3 < epsi) = 0;
    k_seg3 = kb_list_seg3(1:100);
    b_seg3 = kb_list_seg3(101:300);
    knemom_fit_seg3  = mat_lp_seg3(1:end-2*tr_len,:)*kb_list_seg3(1:end);

    res_norm_hist = [res_norm_hist res_norm];
end

[val, ind ] = min(res_norm_hist)
indlist_gen = [indlist_gen ; (6830 + velind_hist)];
indlist_seg3= 6830 + velind_hist;
```

```
figure(3),
subplot 311, plot(knepos_seg3(posind_hist), k_seg3, 'r.-'), title('Segment3
spring values'), axis tight, grid on
subplot 312, plot(knevel_seg3(velind_hist), b_seg3, 'r.-'), title('Segment3
dashpot values1'), axis tight, grid on
subplot 313, plot(1:length(knemom_lp_seg3)-2*tr_len,
knemom_lp_seg3(1:end-2*tr_len) , 'r.',...
    1:length(knemom_lp_seg3)-2*tr_len, knemom_fit_seg3, 'g.','LineWidth',2),
grid on

% Create the fourth linear programming problem (for the fourth segment)

% Segment 4 with -15 degree angular position offset

res_norm_hist = [];
% for offset_seg4 = -25:0
for offset_seg4 = 20
    ind_seg4 = [12615:length(knepos_int) , 1:1050];
    knepos_seg4 = knepos_int(ind_seg4);                    % Impose boundary value
- just for computational purposes
    knepos_seg4_offset = knepos_seg4  - offset_seg4;       % For easier
optimization formulation
    knevel_seg4 = knevel_int(ind_seg4);
    knemom_seg4 = knemom_int(ind_seg4);
    max_knepos_seg4 = max(knepos_seg4_offset);
    min_knepos_seg4 = min(knepos_seg4_offset);

    tr_len = 100;
    knepos_seg4_trial = linspace( min_knepos_seg4, max_knepos_seg4, tr_len);
    delta = abs(knepos_seg4_trial(2) -  knepos_seg4_trial(1));

    knemom_lp_seg4 = zeros(2*tr_len+1,1);
    mat_lp_seg4 = zeros(2*tr_len+1,3*tr_len);

    posind_hist = zeros(tr_len,1);
    velind_hist = zeros(2*tr_len,1);
    for t = 1:tr_len
        [ind1_list] = knepos_seg4_offset > knepos_seg4_trial(t) - delta/2  & ...
            knepos_seg4_offset < knepos_seg4_trial(t) + delta/2 & ...
            knevel_seg4 > 0 ;
        ind1 = find(ind1_list == 1, 1, 'first');
        posind_hist(t) = ind1;
        velind_hist(t) = ind1;

        [ind2_list] = knepos_seg4_offset > knepos_seg4_trial(t) - delta/2  & ...
            knepos_seg4_offset < knepos_seg4_trial(t) + delta/2 & ...
            knevel_seg4 < 0;
        ind2 = find(ind2_list == 1, 1, 'last');
        velind_hist(2*tr_len + 1 - t) = ind2;
    end
    knemom_lp_seg4 = [ knemom_seg4(velind_hist); ...
        knemom_seg4(velind_hist(1:end-1)) -  knemom_seg4(velind_hist(2:end)) ;
0];
    mat_lp_seg4 = [ [ diag(knepos_seg4_offset(posind_hist));
diag(knepos_seg4_offset(posind_hist)) ], ...
        diag(knevel_seg4(velind_hist))];
    mat_lp_seg4 = [mat_lp_seg4 ; [ mat_lp_seg4(1:end-1,:) -
mat_lp_seg4(2:end,:)]];
    mat_lp_seg4 = [mat_lp_seg4 ; 0.2*ones(1,300)];
    options = optimset('MaxIter', 2e3);
    [kb_list_seg4 res_norm res eflag] = lsqlin(mat_lp_seg4, knemom_lp_seg4, [],
[],[],[],zeros(300,1),100*ones(300,1),[],options) ;
    kb_list_seg4(kb_list_seg4 < epsi) = 0;
    k_seg4 = kb_list_seg4(1:100);
    b_seg4 = kb_list_seg4(101:300);
    knemom_fit_seg4  = mat_lp_seg4(1:end-2*tr_len,:)*kb_list_seg4(1:end);

    res_norm_hist = [res_norm_hist res_norm];
end

[val, ind ] = min(res_norm_hist)
indlist_gen = [indlist_gen ; (12615 + velind_hist)];
indlist_seg4 = mod(12615 + velind_hist, length(knemom_int));


figure(4),
subplot 311, plot(knepos_seg4(posind_hist), k_seg4, 'r.-'), title('Segment4
spring values'), axis tight, grid on
subplot 312, plot(knevel_seg4(velind_hist), b_seg4, 'r.-'), title('Segment4
dashpot values1'), axis tight, grid on
```

```
subplot 313, plot(1:length(knemom_lp_seg4)-2*tr_len,
knemom_lp_seg4(1:end-2*tr_len) , 'r.',...
    1:length(knemom_lp_seg4)-2*tr_len, knemom_fit_seg4, 'g.','LineWidth',2),
grid on


start = indlist_gen(indlist_gen > length(knepos_int)) -length(knepos_int) ;
indlist_gen = [start; indlist_gen(1:end-length(start))];
knemom_pas_raw = [knemom_fit_seg1(1:200)' knemom_fit_seg2(1:200)'
knemom_fit_seg3(1:200)' knemom_fit_seg4(1:200)'];
% Smooth
sim('calc_active');
knemom_pas = smooth([knemom_pas(end-1000+1:end)' ;knemom_pas';
knemom_pas(1:1000)'] ,400);
knemom_pas = knemom_pas(1001:end-1000);
knemom_act = smooth(knemom_int - knemom_pas,400)


% Plot the segments
figure(5); cla
hold on
plot(knepos_seg1, knevel_seg1,'r.', 'Linewidth',2)
plot(knepos_seg2, knevel_seg2,'g.', 'Linewidth',2)
plot(knepos_seg3, knevel_seg3,'b.', 'Linewidth',2)
plot(knepos_seg4, knevel_seg4,'m.', 'Linewidth',2)
hold off; grid on; axis square
legend('Segment 1', 'Segment 2' ,'Segment 3', 'Segment 4' ,'Location',
'BestOutside')
xlabel('Angular position (deg)')
ylabel('Angular velocity (deg/s)')

% Plot the experiment data
figure(6); cla
subplot 311, plot(0.01*((1:length(mg.wn2.knepos))-1),mg.wn2.knepos,'k',
'Linewidth',2)
ylabel('Angular position (deg)'), grid on , axis([0 1.37 1.1*min(mg.wn2.knepos)
1.1*max(mg.wn2.knepos)])
subplot 312, plot(0.01*((1:length(mg.wn2.knepos))-1),mg.wn2.knevel,'k',
'Linewidth',2)
ylabel('Angular velocity (deg/s)'), grid on, axis([0 1.37 1.1*min(mg.wn2.knevel)
1.1*max(mg.wn2.knevel)])
```

```
subplot 313, plot(0.01*((1:length(mg.wn2.knepos))-1),mg.wn2.knemom,'k',
'Linewidth',2)
ylabel('Torque (N-m)') , xlabel('time (s)'), grid on, axis([0 1.37
1.1*min(mg.wn2.knemom) 1.1*max(mg.wn2.knemom)])

% Reconstruct

% Get the knepos, knevel and knemom -  interpolate them to 10000 points for
% another walking scenario
knepos_int_tr = smooth(interp([mg.wn4.knepos(end-10+1:end) ; mg.wn4.knepos;
mg.wn4.knepos(1:10)] ,100),len_data_smooth);
knevel_int_tr = smooth(interp([mg.wn4.knevel(end-10+1:end) ; mg.wn4.knevel;
mg.wn4.knevel(1:10)] ,100),len_data_smooth);
knemom_int_tr = smooth( interp([mg.wn4.knemom(end-10+1:end) ; mg.wn4.knemom;
mg.wn4.knemom(1:10)] ,100), len_data_smooth);
hipmom_int_tr = smooth( interp([mg.wn4.lc2(end-10+1:end) ; mg.wn4.lc2;
mg.wn4.lc2(1:10)] ,100), 3*len_data_smooth);
gref_int_tr= smooth( interp([mg.wn4.lc1(end-10+1:end) ; mg.wn4.lc1;
mg.wn4.lc1(1:10)] ,100), 3*len_data_smooth);
knevel_int_tr = knevel_int_tr(1001:end-1000);
knepos_int_tr = knepos_int_tr(1001:end-1000);
knemom_int_tr = knemom_int_tr(1001:end-1000);
hipmom_int_tr = hipmom_int_tr(1001:end-1000);
gref_int_tr = gref_int_tr(1001:end-1000);

sim('decomp_reconstruct')
% smooth knemom_ref
knemom_ref = smooth(knemom_ref(:,2), 5);
plot(knepos_int_tr(1:10:end), knemom_int_tr(1:10:end),'g-', ...
     knepos_int_tr(1:10:end), knemom_ref(1:end-1),'r-','LineWidth',2)
```

3. Three Axis Socket Load Cell Calibration Script

```
%% Three Axis Socket Load Cell Calibartion Script
% Author: Atakan Varol

close all
clear
clc

load('exp_meas_nlc.mat');
% exp_meas2 contains the followin columns:
% mom_sagittal mom_frontal force meas_val1 meas_val2 meas_val3
data(:,6) = data(:,6) - 1.5;

%% Sagittal moment fit

v1 = data(:,5);
v2 = data(:,6);
v3 = data(:,7);
Ms = data(:,2);

A = [ v1.^0 v1.^1 v2.^1 v3.^1];

x_Ms = pinv(A)*Ms;
Ms_est = A*x_Ms;
figure(1);
subplot 311; plot(1:length(Ms),Ms,'r.',1:length(Ms),Ms_est,'g.') ; title('Ms')
subplot 312; plot(1:length(Ms),Ms_est,'r.') ; title('Ms estimated')
subplot 313; plot(1:length(Ms),Ms-Ms_est,'r.') ; title('Ms-Ms estimated')
figure(2);   plot(Ms, Ms_est,'r.' ,-130:130,-130:130,'g-','LineWidth', 2) ;
title('Ms vs Ms estimated'),axis square; grid on
figure(3); bar(x_Ms)
sqmav_Ms = sqrt(mean((Ms - Ms_est).^2))

%% Frontal moment fit

v1 = data(:,5);
v2 = data(:,6);
v3 = data(:,7);
Mf = data(:,3);
```

```
A = [ v1.^0 v1.^1 v2.^1 v3.^1];

x_Mf = pinv(A)*Mf;
Mf_est = A*x_Mf;
figure(4);
subplot 311; plot(1:length(Mf),Mf,'r.',1:length(Mf),Mf_est,'g.') ; title('Mf')
subplot 312; plot(1:length(Mf),Mf_est,'r.') ; title('Mf estimated')
subplot 313; plot(1:length(Mf),Mf-Mf_est,'r.') ; title('Mf-Mf estimated')
figure(5);   plot(Mf, Mf_est,'r.' ,-130:130,-130:130,'g-','LineWidth', 2) ;
title('Mf vs Mf estimated'),axis square; grid on
figure(6); bar(x_Mf)
sqmav_Mf = sqrt(mean((Mf - Mf_est).^2))

%% Ground Reaction force fit

v1 = data(:,5);
v2 = data(:,6);
v3 = data(:,7);
F = data(:,4);

A = [ v1.^0  v2.^1  ];

x_f = pinv(A)*F;
F_est = A*x_f;
figure(7);
subplot 311; plot(1:length(F),F,'r.',1:length(F),F_est,'g.') ; title('F')
subplot 312; plot(1:length(F),F_est,'r.') ; title('F estimated')
subplot 313; plot(1:length(F),F-F_est,'r.') ; title('F-F estimated')
figure(8);   plot(F, F_est,'r.' ,-500:1200,-500:1200,'g-','LineWidth', 2) ;
title('F vs F estimated'),axis square; grid on
figure(9); bar(x_f)
sqmav_F = sqrt(mean((F - F_est).^2))

figure(10)
[v1m,v2m] = meshgrid(-10 : 0.1 : 10, -10 : 0.1 : 10);

res = x_f(1)*1 + x_f(2)*v1m + x_f(3)*v1m.^2 + x_f(4)*v2m + x_f(5)*v2m.^2;
mesh(v1m, v2m, res)
```

APPENDIX B

SIMULINK MODELS

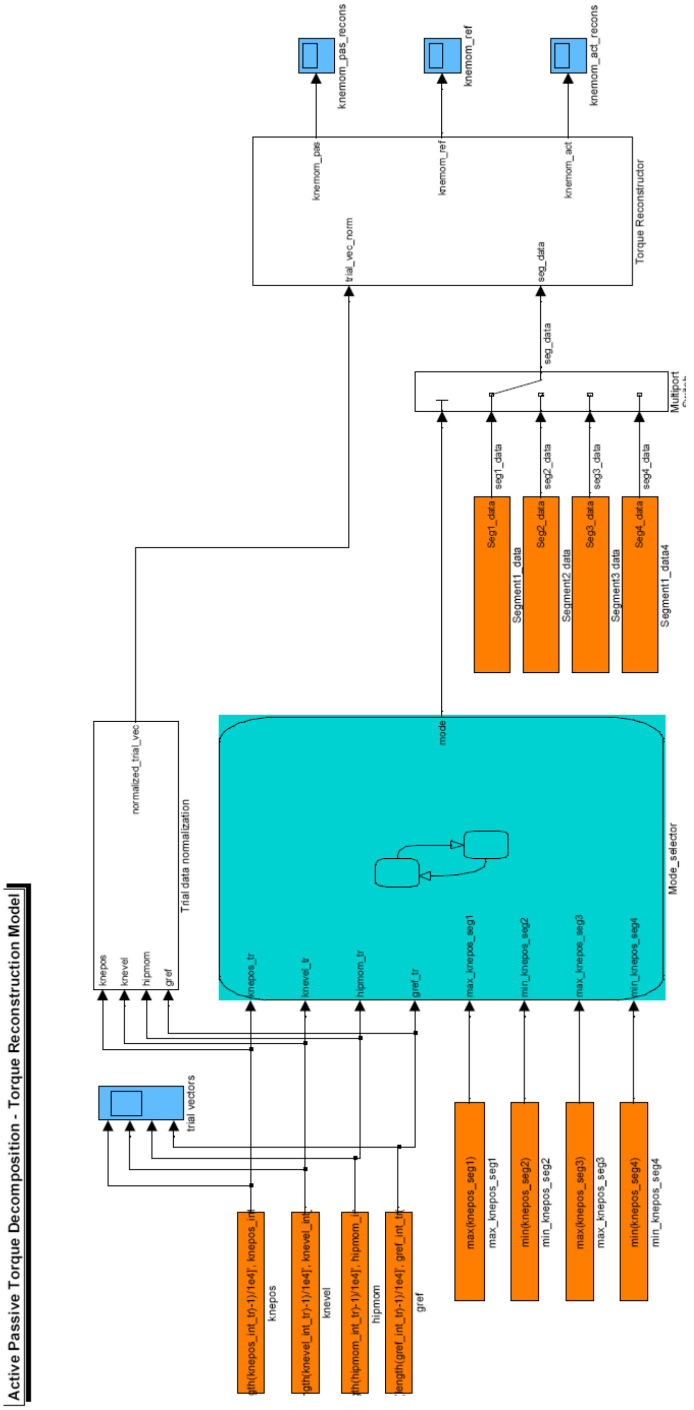

Figure B-1. Active/Passive Torque Decomposition Procedure Torque Reconstruction Main Simulink Block Diagram

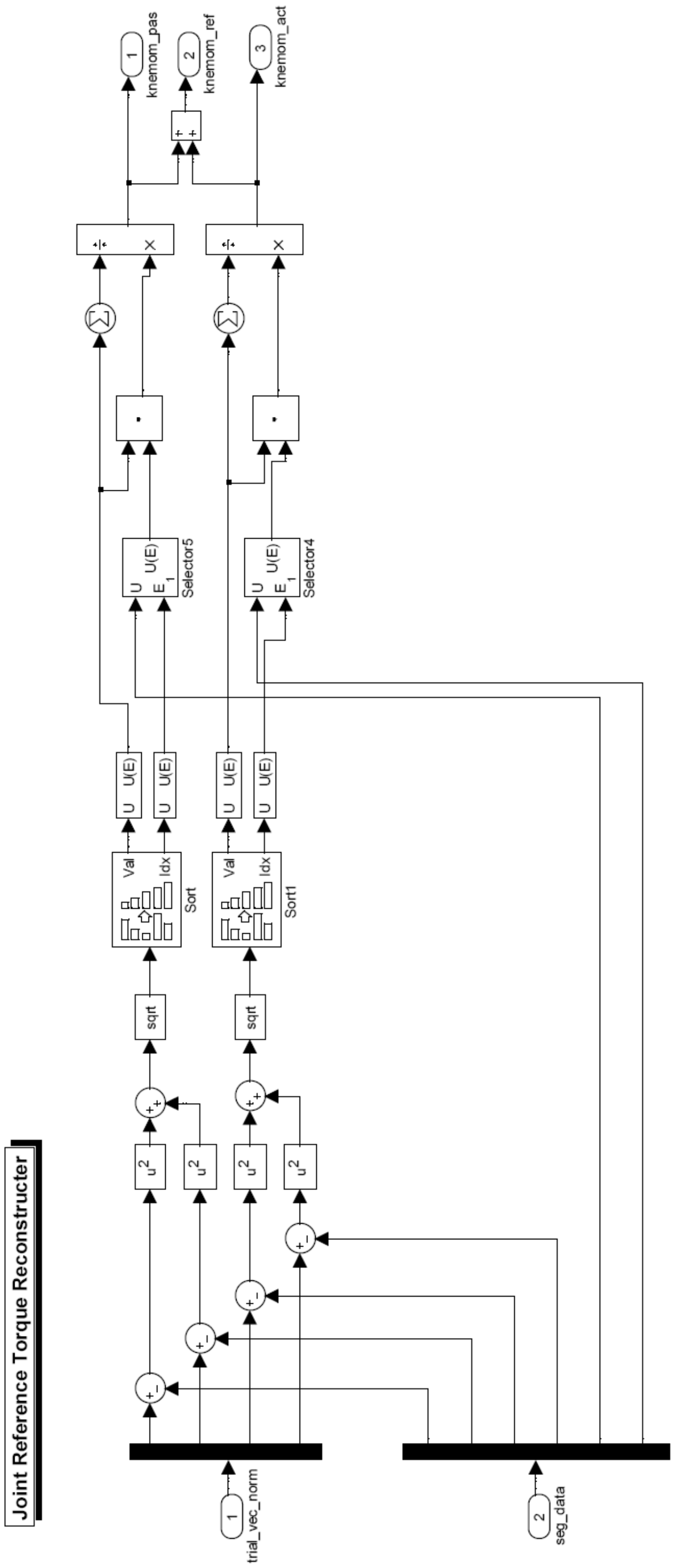

Figure B-2. Joint Torque Reconstructor for the Reconstruction Simulink Block of the Active/Passive Torque Decomposition Procedure.

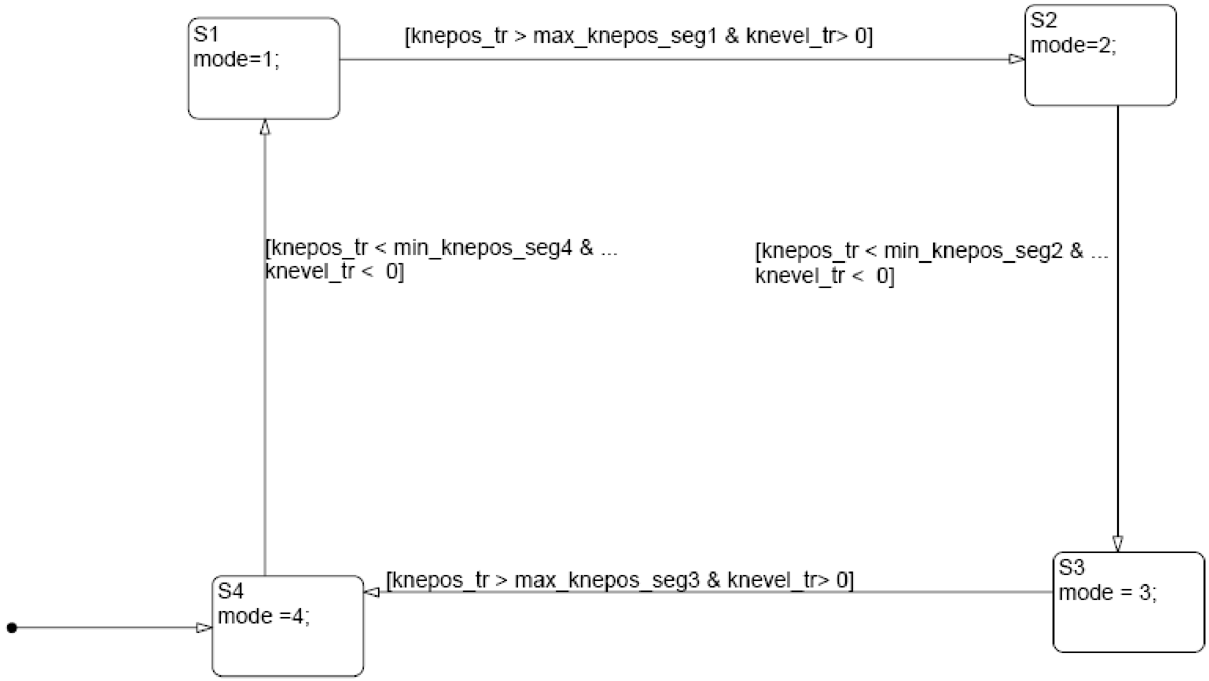
S1
mode=1;
[knepos_tr > max_knepos_seg1 & knevel_tr> 0]
S2
mode=2;
[knepos_tr < min_knepos_seg4 & ...
knevel_tr < 0]
[knepos_tr < min_knepos_seg2 & ...
knevel_tr < 0]
[knepos_tr > max_knepos_seg3 & knevel_tr> 0]
S4
mode =4;
S3
mode = 3;

Figure B-3. Mode Selector for the Reconstruction Simulink Block of the Active/Passive Torque Decomposition Procedure.